EXPERIMENTAL INVESTIGATIONS OF AN ALL-FIBER MULTIREFLECTOR SPECTRAL FILTER FOR OPTICAL COMMUNICATIONS

A Dissertation

by

JONG-SEO LEE

Submitted to the Office of Graduate Studies of
Texas A&M University
in partial fulfillment of the requirements for the degree of

DOCTOR OF PHILOSOPHY

August 2003

Major Subject: Electrical Engineering

EXPERIMENTAL INVESTIGATIONS OF AN ALL-FIBER MULTIREFLECTOR SPECTRAL FILTER FOR OPTICAL COMMUNICATIONS

A Dissertation

by

JONG-SEO LEE

Submitted to Texas A&M University
in partial fulfillment of the requirements
for the degree of

DOCTOR OF PHILOSOPHY

Approved as to style and content by:

Henry F. Taylor
(Chair of Committee)

Ohannes Eknoyan
(Member)

Kai Chang
(Member)

Li Hong Wang
(Member)

Chanan Singh
(Head of Department)

August 2003

Major Subject: Electrical Engineering

ABSTRACT

Experimental Investigations of an All-Fiber Multireflector
Spectral Filter for Optical Communications. (August 2003)

Jong-Seo Lee, B. S., Myong Ji University;
M.S., Texas A&M University
Chair of Advisory Committee: Dr. Henry F. Taylor

All-fiber multireflector spectral filters which have potential application in optical communications have been investigated experimentally. These multireflector etalons were produced by aligning equal-length fiber sections with TiO_2/SiO_2 dielectric mirrors deposited on the end in a silicon v-groove.

Fiber sections 1.33mm in length were produced by polishing, with the fibers held in a silicon wafer polishing jig. The fibers were aligned inside the polishing jig using a precision micro positioner. Then four polishing steps with increasingly finer grit were applied to produce high-quality polished end surfaces on each fiber section. Finally, a dielectric mirror was deposited on one end of each fiber section by magnetron sputtering.

After characterizing the optical loss, length, and mirror reflectance for each of the fiber sections, sections which were well-matched in length were chosen for assembly of the four-mirror etalon, which had nominal reflectance values of 10%, 50%, 50%, and 10% for the dielectric mirrors. Measured transmittance spectra for a mutireflector spectral filter were compared with calculated spectra.

Thermal tuning of the multireflector etalon was also investigated. A 0.34 nm wavelength shift was observed for a 23^0 C temperature change, in agreement with prediction.

To My Lovely Family

ACKNOWLEDGMENTS

I would like to show my sincere appreciation and gratitude to Dr. Henry F. Taylor for his continuous guidance and support, especially for his advice and encouragement throughout my studies at Texas A&M University.

Also, I would like to thank Dr. Ohannes Eknoyan, Dr. Kai Chang, and Dr. Li Hong Wang for providing me with fruitful suggestions and comments on my work and Dr. B. Gregory Cobb as the graduate council representative (GCR) . I would like to thank Mr. Robert Atkinson for good management of the Electro-Optics Lab. Especially, I would also like to express my appreciation to Taehan Bae, Kyungwoo Lee, Xia, and Juan Carlos Juarez.

My deepest gratitude goes to my parents, Mr. Jinkyu Lee and Mrs. Miwha Lee, for their endless love and support. I would like to share this day with my lovely wife Eunchoo Ahn and my daughters Jiyae Lee and JieU Lee, for without their love and patience, this day would not be possible.

TABLE OF CONTENTS

CHAPTER		Page
I	INTRODUCTION	1
II	THEORETICAL REVIEW	5
	A. Interference with Multiple Beams	5
	B. Analysis of the Phase Shift in a Dielectric Mirror and an Etlon	8
	C. Multilayer Dielectric Thin Films	12
III	FABRY PEROT FILTER ANALYSIS	17
	A. Filter Design Assumption	17
	B. Matrix Description of Multi-mirror Etalon	18
	C. Fabry Perot Bandpass Filter	23
IV	DEVICE FABRICATION	26
	A. Silicon Wafer Polishing Jig	26
	B. Coating Materials	31
	C. Coating Thickness of Each Dielectric Thin Film	34
	D. Polishing	37
	E. The Silicon V-groove	40
	F. Setup for Optical Testing of the Filters	44
V	OPTICAL TESTING AND DATA ANALYSIS	48
	A. Characterization of Fiber Sections	48
	B. Characteristics of Multireflector Etalon	58
	C. Temperature Tunning	64
VI	CONCLUSIONS	66
VII	RECOMMENDATIONS	68
REFERENCES		69
APPENDIX 1		74

Page

APPENDIX 2 79

VITA 80

LIST OF TABLES

TABLE		Page
I	Calculated reflectances for etalon with flat-top response and zero Reflectance at the center of the transmittance band	21
II	The characteristics of some coating materials	32
III	Specifications of the silicon v-grooves	42
IV	Characteristics of fiber sections	51

LIST OF FIGURES

FIGURE		Page
1	Dependence of optical transmittance T on optical frequency ν for an ideal filter for optical communication	2
2	Multireflector etralon to achieve near-ideal transmittance characteristics	3
3	Transmittance spectra calculated for etalons with 2, 4, and 6 equally spaced mirrors. In these examples, reflectance values are $R_1 = R_2 = .962$ for N = 2; $R_1 = R_4 = .695$, $R_2 = R_3 = .984$ for N = 4; and $R_1 = R_6 = .448$, $R_2 = R_5 = .941$, and $R_3 = R_4 = .981$ for N = 6	3
4	Spectra in Fig. 3 plotted with expanded frequency scale	4
5	Fabry Perot interferometer, with mirror reflectance R and cavity length L, with $\mathbf{E_i}$ the incident electric amplitude and $\mathbf{E_t}$ the transmitted electric field amplitude	5
6	An interface between dielectric media	9
7	A simple dielectric thin film structure	10
8	Two thin film reflectors in series	11
9	A multilayer dielectric thin film stack	12
10	Electric fields illustration on a single thin film layer	13
11	Illustration of electric field amplitudes and propagation phase shift between adjacent mirrors	18
12	Calculated transfer fuction for R1,R4 =10% and R2,R3 = 51.17%	22

FIGURE Page

13 The power transfer function of two reflector Fabry Perot filter 24
14 Three major Miller planes of silicon 27
15 Silicon wafers with two different orientations 27
16 A polishing jig after grooving on the silicon wafer 29
17 A silicon wafer with a fiber positioned in a groove 30
18 A polishing jig with top cover in place 30
19 Deposition techniques 33
20 Refractive indices of TiO_2 and SiO_2 34
21 Dependence of reflectance on film thickness for a film of index n_2=2.3 sandwiched between regions of index n_1=n_3=1.46 36
22 A diagram of aligning a fiber in the polishing jig 37
23 69-3000 FIBRMET optical fiber polisher from Beuhler Ltd. 38
24 A diagram of the silicon v-groove 41
25 Aligning fibers inside the silicon v-groove 43
26 The optical test setup 44
27 Fibers inside the silicon v-groove 45
28 The experimental setup 46
29 ASE output Spectrum 47
30 Transmittance spectrum for a single fiber section with a 10% mirror on one end and a Fresnel reflection of 3.6% from the other end 49
31 Transmittance spectrum of fiber section 1 with, R=9.6% 52
32 Transmittance spectrum of fiber section 2 with, R=9.5% 52
33 Transmittance spectrum of fiber section 3 with, R=9.6% 53

FIGURE Page

34 Transmittance spectrum of fiber section 4 with, R=10.6% 53
35 Transmittance spectrum of fiber section 1 with, R=49% 54
36 Transmittance spectrum of fiber section 2 with, R=49.6% 54
37 Transmittance spectrum of fiber section 3 with, R=48.6% 55
38 Transmittance spectrum of fiber section 4 with, R=51.3% 55
39 Visibility test of a fiber with a 9.6% reflector on one end 56
40 Visibility test of a fiber with a 49% reflector on one end 57
41 Transmission spectra for N=2,3, and 4 over the C-band (1530-1560nm) 58
42 Transmission spectra for N=3 and 4, with optical power plotted on a logarithmic scale 59
43 The transmission spectrum without index matching 60
44 Comparison between calculated and observed transmittance spectra for N=4 61
45 A transmission spectrum over entire C-band (1530-1560nm) 62
46 Measured transmission and reflection spectra for four-mirror etalon 63
47 Temperature tuning of the spectral response 65

CHAPTER I

INTRODUCTION

Recently, the interest in all-fiber spectral filters has increased due to their potential application in telecommunications and sensing. In particular, such filters are needed for dense wavelength division multiplexing (DWDM) in optical fiber communication networks to provide greater channel density over the available carrier frequency bandwidth [1].

Two types of optical fiber filters are in general use. The fiber Bragg grating (FBG) is based on a spatially periodic refractive index variation in the fiber. The reflectance spectrum of the FBG filter is characterized by a single narrow peak with side lobes, and thus can be used as a bandpass filter [2]. The two mirror Fiber Fabry-Perot Interferometer (FFPI) makes use of discrete reflectors to form a resonant cavity. The transmittance spectrum is periodic in frequency, and is characterized by sharp peaks at the resonance frequencies [2,3,4]. The separation between the transmittance peaks in frequency is known as the free spectral range FSR. Practical two mirror FFPI filters make use of a cavity formed by an air gap between two dielectric mirrors [5,6].

An ideal spectral filter for optical communication would have flat in-band response and no out-of-band response, as in Fig. 1. Two mirror FFPI filters are not very close to this ideal, due to the gradual (6 dB/octave) drop off in transmittance with frequency away from the peaks.

Journal model is *IEEE Journal of Lightwave Technology.*

A response characteristic which is closer to the ideal of Fig. 1 would allow for closer channel spacing in DWDM systems [5].

Previous studies have shown that multimirror etalons with N equally spaced reflectors (N >2), as in Fig. 2, can have response characteristics closer to the ideal than the two-mirror FFPIs [5,7]. In these designs, the mirror reflectance values are tapered, with higher reflectances near the center. As the plots in Figs. 3 and 4 show, the spectra approach the ideal of Fig. 1 as the number of reflectors increases [8].

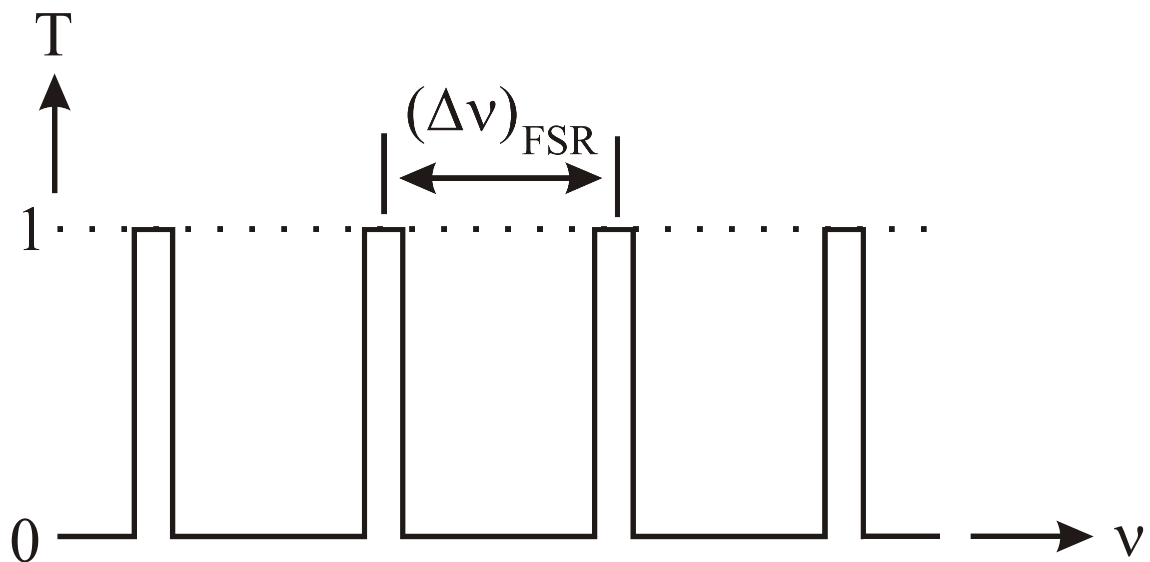

Fig. 1. Dependence of optical transmittance T on optical frequency ν for an ideal filter for optical communication.

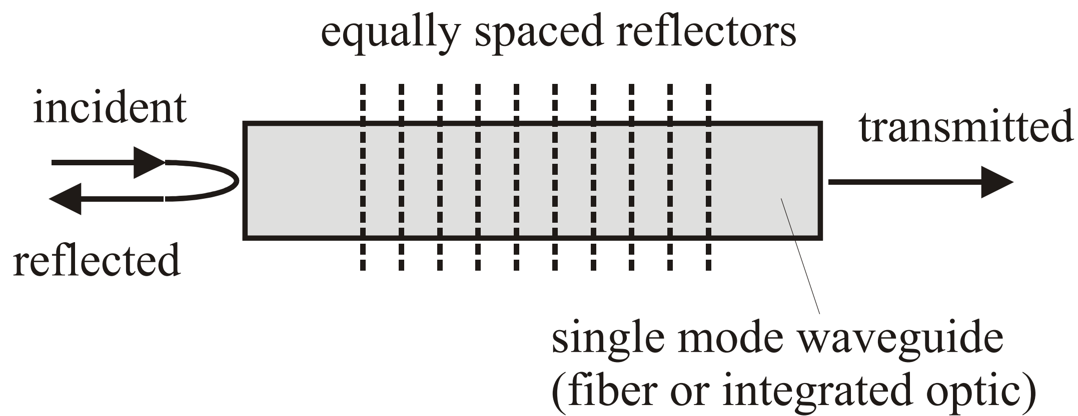

Fig. 2. Multireflector etalon to achieve near-ideal transmittance characteristics.

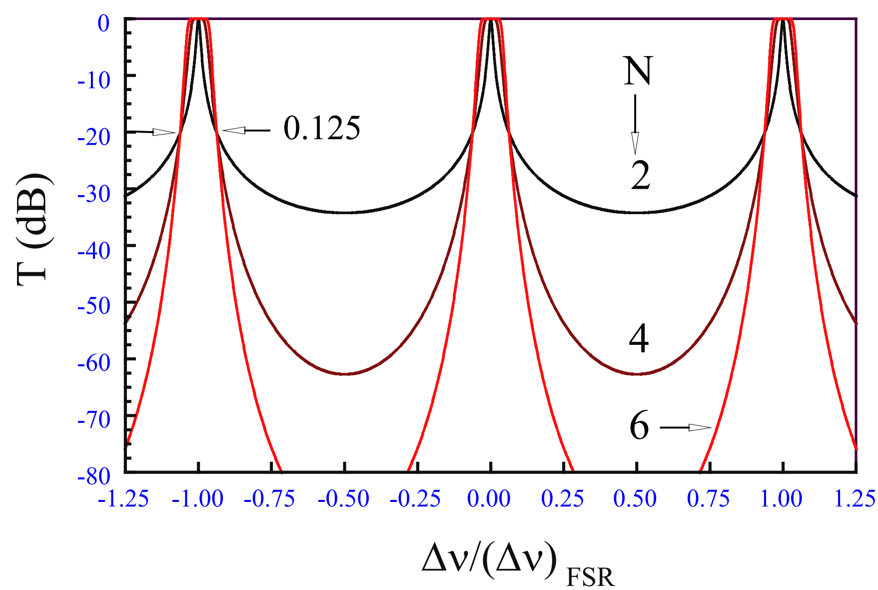

Fig. 3. Transmittance spectra calculated for etalons with 2, 4, and 6 equally spaced mirrors. In these examples, reflectance values are $R_1 = R_2 = .962$ for N = 2; $R_1 = R_4 = .695$, $R_2 = R_3 = .984$ for N = 4; and $R_1 = R_6 = .448$, $R_2 = R_5 = .941$, and $R_3 = R_4 = .981$ for N = 6.

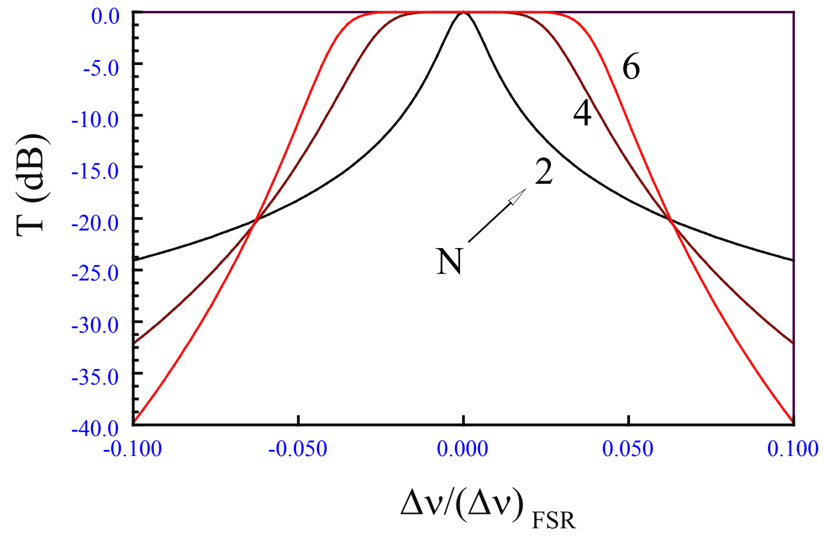

Fig. 4. Spectra in Fig. 3 plotted with expanded frequency scale.

CHAPTER II

THEORETICAL REVIEW

A. Interference with Multiple Beams

A two mirror Fabry Perot interferometer, also called an etalon, consists of two partially reflecting mirrors separated by a distance L [9]. When coherent light from a laser is launched into an etalon, the light reflects back and forth between these two reflectors, as illustrated in Fig. 5. The highest quality reflectors are multilayer dielectrics such as alternate SiO_2/TiO_2 layers deposited on glass substrates [10].

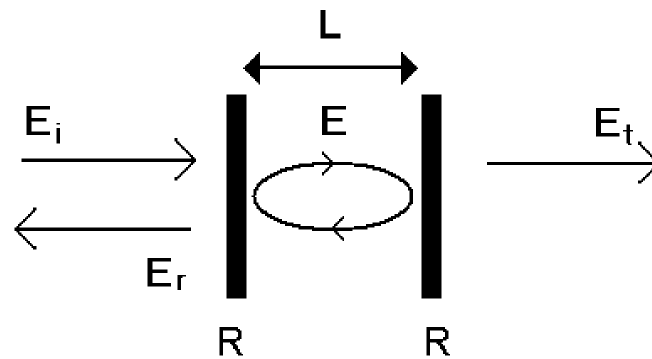

Fig. 5. Fabry Perot interferometer, with mirror reflectance R and cavity length L, with $\mathbf{E_i}$ the incident electric amplitude and $\mathbf{E_t}$ the transmitted electric field amplitude.

The amplitude of the electric field of the light leaving the etalon is $\mathbf{E_t}$. If we consider that no light is present initially and the incident wave of amplitude $\mathbf{E_i}$ is turned on at a time t=0, then the field **E** just to the right of the first mirror is given by

$$E = t\,E_i \tag{1}$$

with *t*, the amplitude transmission coefficient given by

$$t = \sqrt{1-R} \tag{2}$$

This light initially entering the etalon proceeds through the cavity to the second mirror, where it is partially reflected and experiences a reduction in amplitude by a factor *r*, the amplitude reflection coefficient, given by

$$r = \sqrt{R} \tag{3}$$

The once-reflected light then travels in the backwards direction until it encounters the first mirror, where it is partially reflected again and experiences another attenuation in amplitude by a factor r.

In traveling through the cavity twice, the light also experiences a round trip phase shift δ [11], given by

$$\delta = \frac{4\pi\, n\, L}{\lambda}, \tag{4}$$

with *n* the refractive index of the medium between the mirrors and λ the the free-space optical wavelength.

Thus, after the light $\mathbf{E_i}$ has been turned on long enough for it to make one round trip in the cavity, the amplitude **E** has become

$$E = E_i t + E_i t r^2 e^{i\delta} \tag{5}$$

Here, it is assumed that no loss due to scattering or absorption is experienced by the light propagating in the cavity. Using the same argument, after M round trips we can write

$$E = E_i t \sum_{M=0}^{M} a^m \quad (6)$$

with $a = r^2 e^{i\delta}$. In the steady state, $M \to \infty$,

$$E_t = \frac{E_i t^2}{1 - r^2 e^{i\delta}} \quad (7)$$

where use has been made of the result that, if $|a| < 1$, $\sum_{M=0}^{\infty} a = \frac{1}{1-a}$, and that $E_t = tE$. The transmittance T is given by $T = \frac{|E_t|^2}{|E_i|^2}$, and it follows from equations (3) and (7) that

$$T = \frac{(1-R)^2}{1 + R^2 - 2R\cos\delta} \quad (8)$$

Phase shifts not only occur inside an etalon but also at each reflector. The coefficient of reflection and transmission are defined as amplitude ratios, that is

$$r = \frac{E_r}{E_i} \quad (9)$$

$$t = \frac{E_t}{E_i} \quad (10)$$

where E_i is the amplitude of the incident light, E_r is the amplitude of the reflected light, and E_t is the amplitude of the transmitted light.

These amplitude coefficients can be written, if the light is incident in a medium of refractive index n1 in the form normal to an interface with a medium of index n2,

$$r = \frac{n_1 - n_2}{n_1 + n_2} \tag{11}$$

$$t = \frac{2n_1}{n_1 + n_2} \tag{12}$$

From equation (11), if the incident medium has lower refractive index than the transmitting medium, the amplitude reflection coefficient has a negative value which means a π radian phase shift. On the other hand, if the incident medium has higher refractive index than the transmitting medium, the amplitude reflection coefficient has a positive value, or 0 radian phase shift.

The amplitude transmission coefficient always has a positive value, which means when light passes through the interface between two different media, no phase shift occurs.

B. Analysis of the Phase Shift in a Dielectric Mirror and an Etalon

Consider light incident in a medium of refractive index n_1, which is partially reflected at an interface with a medium of index n_2, as shown in Fig. 6.

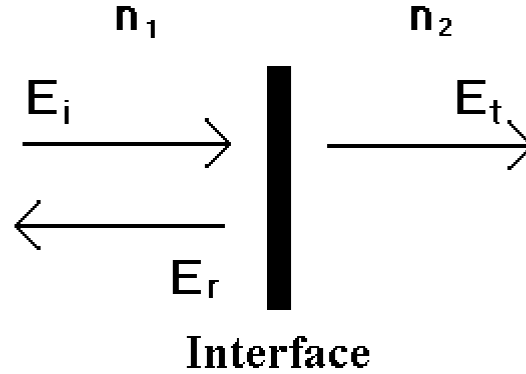

Fig. 6. An interface between dielectric media.

As mentioned in previous section, the amplitude reflection coefficient at this interface is

$$r = \frac{E_r}{E_i} = \frac{n_1 - n_2}{n_1 + n_2} \tag{13}$$

Let $r = \left|\frac{n_1 - n_2}{n_1 + n_2}\right|$, then $\frac{E_r}{E_i} = r$ if $n_1 > n_2$, no phase shift

$\frac{E_r}{E_i} = -r$ if $n_1 < n_2$, π-rad phase shift

In either case, the amplitude transmission coefficient , $\frac{E_t}{E_i} = \sqrt{1 - r^2}$, has no phase shift.

Now consider a film of a refractive index n_2 with thickness *t* between semi-infinite media of index n_1, as shown in Fig. 7.

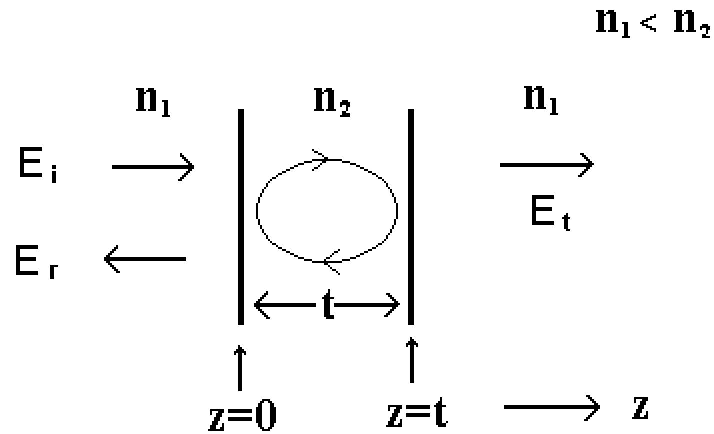

Fig. 7. A simple dielectric thin film structure.

In the plane z=0, the amplitude reflection coefficient is $-r$ because the refractive index of the incident medium is less than that of the transmitting medium. This means that a π radian phase shift occurs at the first interface. If the thickness of the thin film is a quarter wavelength of the light in the film,

$$t = \frac{\lambda}{4n_2} \tag{14}$$

then in the plane z=0, the amplitude reflection coefficient is $-r$ from the second interface after a round trip inside the film.

The round trip phase shift from equation (4) in the thin film is

$$\delta = \frac{4\pi n_2 t}{\lambda} = \frac{4\pi}{4} = \pi \tag{15}$$

The total phase shift at the first interface, z=0, is reflection phase shift (at z=0) + propagation phase shift in film + reflection phase shift (at z=t) which is π + π + 0, respectively. Thus, the total phase shift in phase z=0, considering both

interfaces, is $\frac{E_r}{E_i} = -2r =$ 2π radians phase shift, where "– "sign indicates π radians phase shift so, "-2" indicates 2π radians phase shift. Now consider two such reflection in series, with an index profile given by Fig.8.

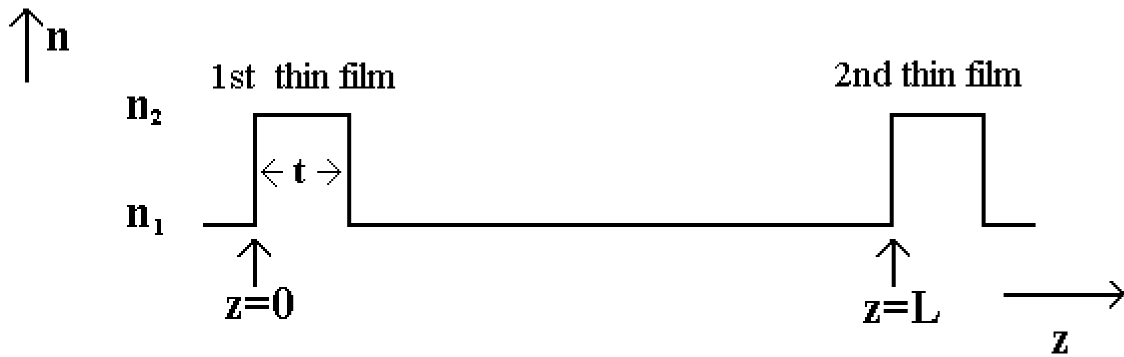

Fig. 8. Two thin film reflectors in series.

For the maximum transmission of the light, the reflection should be a minimum in the plane z=0. For this to occur, the reflected field amplitude from mirror 2 must be 180° out of phase relative to the reflection from mirror 1 in the plane z=0.

This requires that the one-way propagation phase shift from z=0 to z=L is given by

$$\phi = \frac{2\pi n_2 t}{\lambda} + \frac{2\pi n_1 (L-t)}{\lambda} = (m + \frac{1}{2})\pi \qquad (16)$$

where n_1 is the refractive index of a material inside the etalon, n_2 is the refractive index of the thin film, and m is an integer.

Therefore, the round trip propagation phase shift from z=0 to z=L to obtain the maximum transmission is $2\phi = (2m + 1)\pi$.

Thus, the conclusion is that the phase shift between the centers of two adjacent mirrors, $\phi = (m + \frac{1}{2})\pi$, gives zero reflectance and maximum transmittance.

C. Multilayer Dielectric Thin Films

Multilayer dielectric thin films are used in many applications [12, 13], including fiber Fabry Perot etalons [14]. Multilayer films, which produce much higher reflectance than a single-layer film [10], are usually deposited on a well prepared end of a fiber surface by magnetron sputtering [15]. In order to obtain a high value of reflectance in a multiplayer thin film, the thickness of each layer should be a quarter of the wavelength of the light in the layer [16].

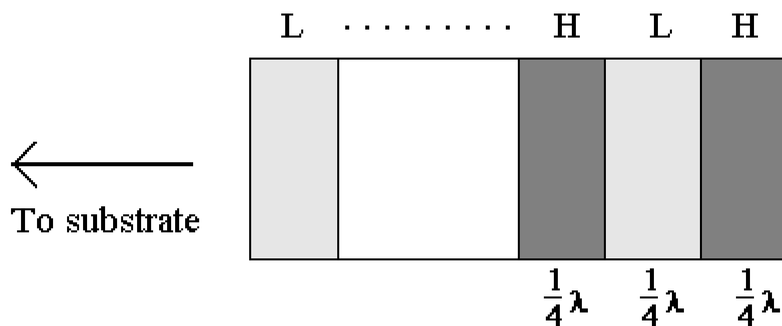

Fig. 9. A multilayer dielectric thin film stack.

The transfer matrix method is used for analyzing multiplayer dielectric thin films [17]. A multilayer and single layer dielectric thin film structure is illustrated in Fig.9. and Fig. 10. respectively.

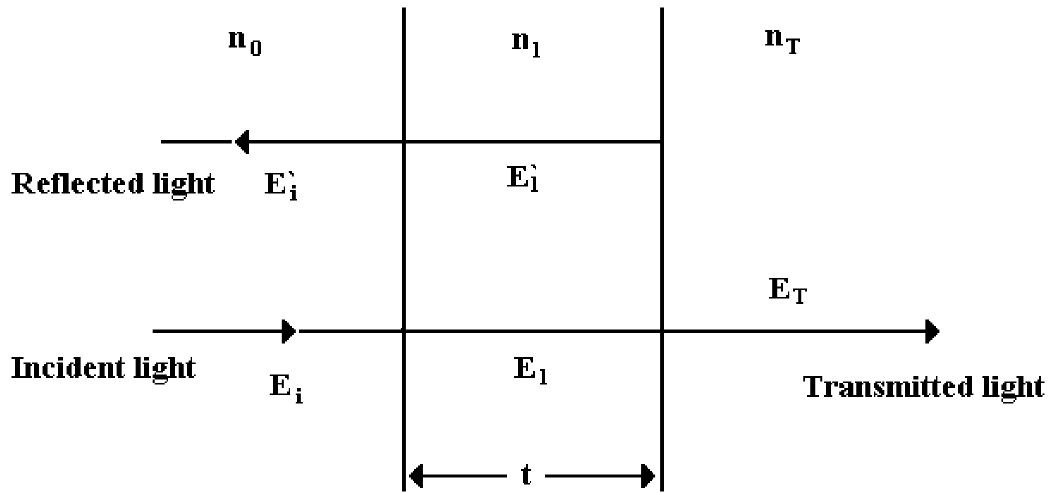

Fig. 10. Electric fields illustration on a single thin film layer.

Let **E** and **E`** denote the amplitudes of the transmitted and reflected light, respectively. The relation between reflected and transmitted electric field amplitudes is given by

$$\begin{bmatrix} 1 \\ n_0 \end{bmatrix} + \begin{bmatrix} 1 \\ -n_0 \end{bmatrix} \frac{E_0`}{E_0} = \begin{bmatrix} \cos kl & \frac{-i}{n_1}\sin kl \\ -in_1 \sin kl & \cos kl \end{bmatrix} \begin{bmatrix} 1 \\ n_T \end{bmatrix} \frac{E_T}{E_0} \tag{17}$$

which can be written as

$$\begin{bmatrix} 1 \\ n_0 \end{bmatrix} + \begin{bmatrix} 1 \\ -n_0 \end{bmatrix} r = M \begin{bmatrix} 1 \\ n_T \end{bmatrix} t \tag{18}$$

where is r the amplitude reflection coefficient, t is the amplitude transmission coefficient, and M is known as the transfer matrix which is given by

$$M = \begin{bmatrix} \cos kl & \frac{-i}{n_1}\sin kl \\ -in_1 \sin kl & \cos kl \end{bmatrix} \tag{19}$$

where $k = \frac{2\pi n_1}{\lambda_0}$.

With this transfer matrix, N layer thin films can be analyzed, in which indices of refraction $n_1, n_2, n_3, \ldots n_N$ and thicknesses $l_1, l_2, l_3, \ldots l_N$, respectively. The amplitude reflection and transmission coefficients of the multilayer thin film are given by

$$\begin{bmatrix} 1 \\ n_0 \end{bmatrix} + \begin{bmatrix} 1 \\ -n_0 \end{bmatrix} r = M_1 M_2 M_3 \cdots M_N \begin{bmatrix} 1 \\ n_T \end{bmatrix} t \tag{20}$$

where the transfer matrices of the each layer are denoted by $M_1 M_2 M_3 \cdots M_N$. Each transfer matrix has their proper values of n,l, and k. The overall transfer matrix M is the product of the individual transfer matrices.

$$M_1 M_2 M_3 \cdots M_N = M = \begin{bmatrix} A & B \\ C & D \end{bmatrix} \tag{21}$$

Solving the equation (20) for r and t in terms of these elements, the amplitude reflectance and transmission coefficients for the multilayer dielectric thin film are given by

$$r = \frac{An_0 + Bn_T n_0 - C - Dn_T}{An_0 + Bn_T n_0 + C + Dn_T} \tag{22}$$

$$t = \frac{2n_0}{An_0 + Bn_T n_0 + C + Dn_T} \tag{23}$$

Therefore, we can calculate the reflectance R and transmittance T, respectively, to be

$$R = |r|^2 \; and \;\; T = |t|^2 \tag{24}$$

For 3 layer dielectric thin film reflector which consists of TiO_2 and SiO_2, successively of alternating layers, the refractive indices of each layer are n_1=2.3, n_2=1.46, n_3=2.3, and n_0=1.46 and n_T=1.46 [12]. Also, each layer has a quarter wavelength thickness, 1685Å for TiO_2 and 2654Å for SiO_2, respectively at λ_0 =1550 nm. That is l_1=1685 Å, l_2=2654 Å, and l_3=1685 Å.

Using equation (19), each transfer matrix M_1, M_2, and M_3 is given by

$$M_1 = \begin{bmatrix} \cos k_1 l_1 & \frac{-i}{n_1}\sin k_1 l_1 \\ -in_1 \sin k_1 l_1 & \cos k_1 l_1 \end{bmatrix} \tag{25}$$

$$M_2 = \begin{bmatrix} \cos k_2 l_2 & \frac{-i}{n_2}\sin k_2 l_2 \\ -in_2 \sin k_2 l_2 & \cos k_2 l_2 \end{bmatrix} \tag{26}$$

$$M_3 = \begin{bmatrix} \cos k_3 l_3 & \frac{-i}{n_3}\sin k_3 l_3 \\ -in_3 \sin k_3 l_3 & \cos k_3 l_3 \end{bmatrix} \tag{27}$$

Since first and third layer are same, then transfer matrix M_1 equals to M_3.

Solving equation (21) can get A = D relationship which is

$$A = \left(\cos^2(k_1 l_1) - \sin^2(k_1 l_1)\right)\cos(k_2 l_2) - \left(\left(\frac{n_2}{n_1} + \frac{n_1}{n_2}\right)\cos(k_1 l_1)\sin(k_1 l_1)\sin(k_2 l_2)\right) \tag{28}$$

$$B = -2\frac{i}{n_1}\sin(k_1 l_1)\cos(k_1 l_1)\cos(k_2 l_2) - i\left(\frac{1}{n_2}\cos^2(k_1 l_1) - \frac{n_2}{n_1^{\,2}}\sin^2(k_1 l_1)\right)\sin(k_2 l_2) \tag{29}$$

$$C = -2i\sin(k_1 l_1)\cos(k_1 l_1)\cos(k_2 l_2) - i\left(n_2\cos^2(k_1 l_1) - \frac{n_1^{\;2}}{n_2}\sin^2(k_1 l_1)\right)\sin(k_2 l_2) \tag{30}$$

The total reflectance of a 3 layer thin film is 0.5172 (51.72%) after solving equation (22) for calculated elements A, B, C, and D of the transfer matrix with n_0=1.46, and n_T =2.3.

CHAPTER III

FABRY PEROT FILTER ANALYSIS

A. Filter Design Assumption

The filter analyzed in this paper consists of N-1 sections of a single mode optical waveguide separated by N equally spaced, lossless mirrors of reflectance Rj, j=0,1,2,….N-1. The length of the sections, measured between the centers of adjacent mirrors, is *L*.

The propagation phase shift between adjacent mirrors ϕ is given by

$$\phi = \frac{2\pi\nu\, nL}{c} \tag{31}$$

at a frequency ν, with *n* the effective refractive index of the waveguide mode and c the free-space speed of light. The filter is designed to have a transmittance of 1 at frequencies ν_m, with *m* a positive integer. It will be assumed that

$$\phi_m = (m + \frac{1}{2})\pi \tag{32}$$

with ϕ_m the propagation phase shift between mirrors at frequency ν_m. This design assumption ensures that reflected waves from adjacent mirrors are 180° out of phase.

B. Matrix Description of Multi-mirror Etalon

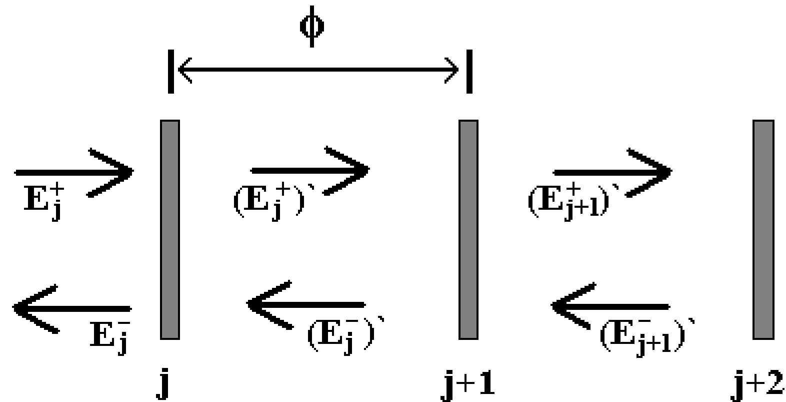

Fig.11. Illustration of electric field amplitudes and propagation phase shift between adjacent mirrors.

The transmittance of a thin-film assembly is independent of the direction of propagation of the light. The matrix approach to the analysis of mulireflector etalons was introduced by Taylor [8]. The model for analyzing the multireflector uses the expression

$$\mathbf{E}_{\mathrm{j}} = \mathbf{M}_{\mathrm{j}}\mathbf{E}_{\mathrm{j+1}} \tag{33}$$

to calculate the effect of a mirror of reflectance R_j . The value of ϕ_m the propagation phase shift between two adjacent reflectors at a resonant wavelength λ_m is given by

$$\phi_m = \frac{2\pi nL}{\lambda_m} = (m + \frac{1}{2})\pi \tag{34}$$

where for maximum transmittance T=1.

The vector $\mathbf{E}_{\mathrm{j}}$ is given by

$$\mathbf{E}_j = \begin{bmatrix} \mathbf{E}_j^+ \\ \mathbf{E}_j^- \end{bmatrix} \tag{35}$$

where $\mathbf{E}_j^+$ and $\mathbf{E}_j^-$ are the forward and reverse propagating electric field amplitudes just prior to mirror j, and $\mathbf{M}_j = \mathbf{M}_j^R \mathbf{M}^\varphi$, for j = 0,1,…,N-1.

Electric field components for the incident and reflected waves are illustrated in Fig. 11. The matrix $\mathbf{M}_j^R$ represents the effect of reflection at the j'th mirror. The matrix $\mathbf{M}^\varphi$, which represents the effect of light propagating between adjacent mirrors, is given by

$$\mathbf{M}^\varphi = \begin{bmatrix} \mathbf{e}^{-i\varphi} & \mathbf{0} \\ \mathbf{0} & \mathbf{e}^{i\varphi} \end{bmatrix} \tag{36}$$

where ϕ the phase shift for light traveling between mirrors j and j+1 at frequency ν.

Assuming a $\frac{\pi}{2}$ radian phase shift for a reflected wave and no phase shift for the transmitted wave, the fields on either side of the mirror are related by

$$(\mathbf{E}_j^+)' = \sqrt{\mathbf{1} - \mathbf{R}_j}\,\mathbf{E}_j^+ + \mathbf{i}\sqrt{\mathbf{R}_j}\,(\mathbf{E}_j^-)' \tag{37}$$

$$\mathbf{E}_j^- = \sqrt{\mathbf{1} - \mathbf{R}_j}\,(\mathbf{E}_j^-)' + \mathbf{i}\sqrt{\mathbf{R}_j}\,\mathbf{E}_j^+ \tag{38}$$

The reflectance matrix R_N for N mirrors in series, separated by identical phase-shift regions, is given by

$$\mathbf{R}_N = \left(\prod_{j=0}^{N-2} \mathbf{M}_j^R \mathbf{M}^\varphi \right) \mathbf{M}_{N-1}^R \tag{39}$$

The transmittance T and reflectance R are defined respectively,

$$\mathbf{T} = \frac{\mathbf{1}}{\left|\mathbf{E}_0^+\right|^2} \tag{40}$$

$$\mathbf{R} = \frac{\left|\mathbf{E}_0^-\right|^2}{\left|\mathbf{E}_0^+\right|^2} \tag{41}$$

The boundary conditions are $\mathbf{E}_N^+ = \mathbf{1}$ and, since no wave enters the etalon from the right, $\mathbf{E}_N^- = \mathbf{0}$. The relationship between incident and transmitted electric fields is

$$\begin{bmatrix} \mathbf{E}_0^+ \\ \mathbf{E}_0^- \end{bmatrix} = \mathbf{R}_N \begin{bmatrix} \mathbf{E}_N^+ \\ \mathbf{E}_N^- \end{bmatrix} \tag{42}$$

Since $\mathbf{E}_N^+ = \mathbf{1}$ and $\mathbf{E}_N^- = \mathbf{0}$, equation (42) can be written

$$\begin{bmatrix} \mathbf{E}_0^+ \\ \mathbf{E}_0^- \end{bmatrix} = \mathbf{R}_N \begin{bmatrix} 1 \\ 0 \end{bmatrix} \tag{43}$$

So, $\mathbf{E}_0^+ = \mathbf{R}_N$. Therefore, the transfer function for multi-reflector etalon is defined as,

$$\mathbf{T} = \frac{\mathbf{1}}{\left|\mathbf{R}_N\right|^2} \tag{44}$$

For N=4, the reflectance values which give a zero reflectance at band pass and flat-top response are calculated from (45), (46), and (47) [8]. Numerical results are summarized in Table 1.

$$\zeta_j = \tanh^{-1}(\sqrt{R_j}) \tag{45}$$

$$\zeta_3 = \zeta_0, \quad \zeta_2 = \zeta_1 \tag{46}$$

$$2\zeta_1 - 2\zeta_0 - \sinh^{-1}\left(2\sinh(2\zeta_0)\right) = 0 \tag{47}$$

Table 1. Calculated reflectances for etalon with flat-top response and zero reflectance at the center of the transmittance band.

R1 and R4 (%)	R2 and R3 (%)
7	41.01
8	44.7
9	48.07
10	51.17
11	54.02
12	56.65

The etalon transmittance characteristic is given in Fig. 12 using the reflectance values 10% (R1,R4) and 51.17% (R2, R3).

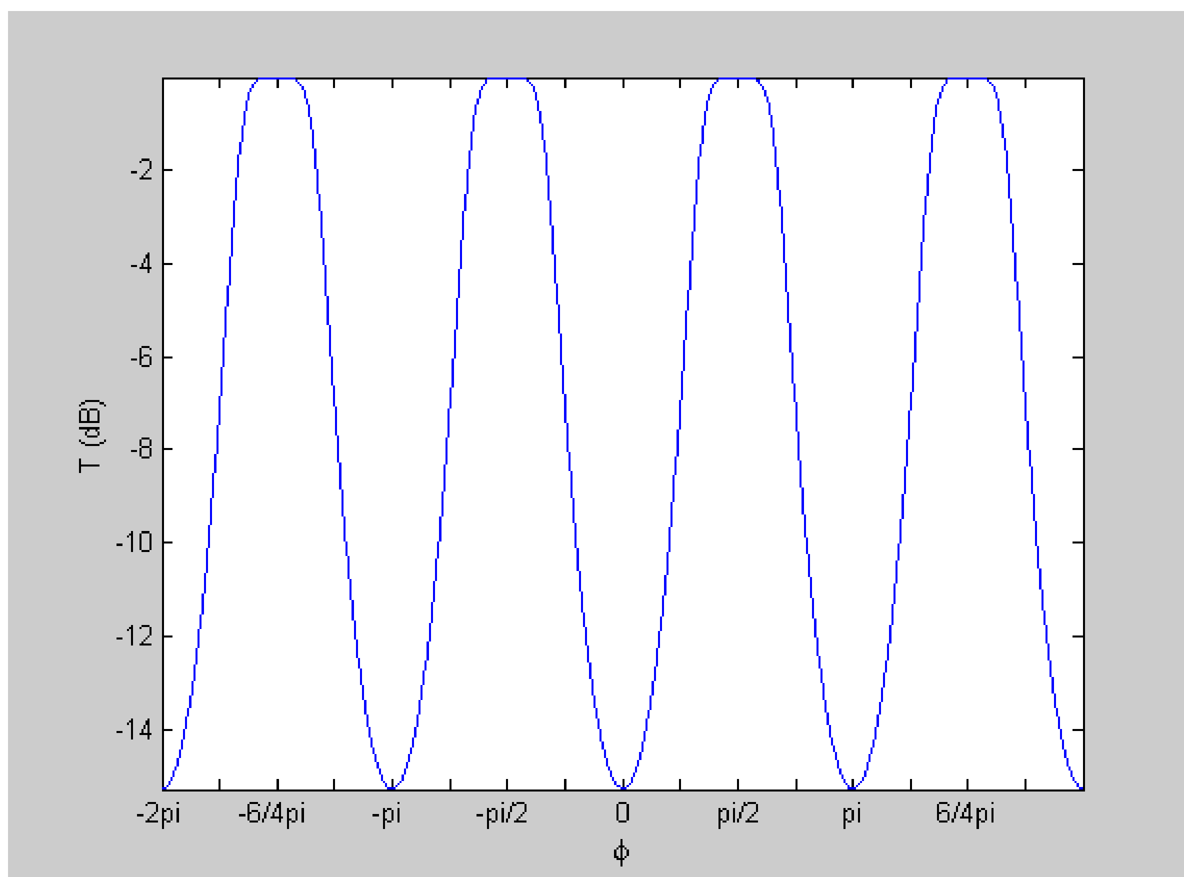

Fig. 12. Calculated transfer function for R1, R4 = 10% and R2, R3=51.17%.

C. Fabry Perot Bandpass Filter

The transmittance T of the lossless two mirror Fabry Perot filter is given from equation (8) by

$$\mathbf{T} = \frac{(1-R)^2}{1+R^2-2R\cos(4\pi\nu\tau)} \tag{48}$$

where R is the reflectance of each of the mirrors, and $4\pi\nu\tau$ is the round-trip optical phase shift in the cavity. Alternately, the transmittance can be written as

$$\mathbf{T} = \frac{(1-R)^2}{(1-R^2)+R(2\sin(2\pi\nu\tau))^2} \tag{49}$$

which can be obtained by use of the trigonometric double angle formula which is,

$$\cos 2x = 1-\sin^2 x \tag{50}$$

Equation (49) can be written as

$$\mathbf{T} = \frac{1}{1+\left(\frac{2\sqrt{R}}{1-R}\sin(\frac{4\pi\nu\tau}{2})^2\right)} \tag{51}$$

This right hand side is known as Airy function [18] and the transmittance characteristic (51) is plotted in Fig.13 for different values of the mirror reflectance.

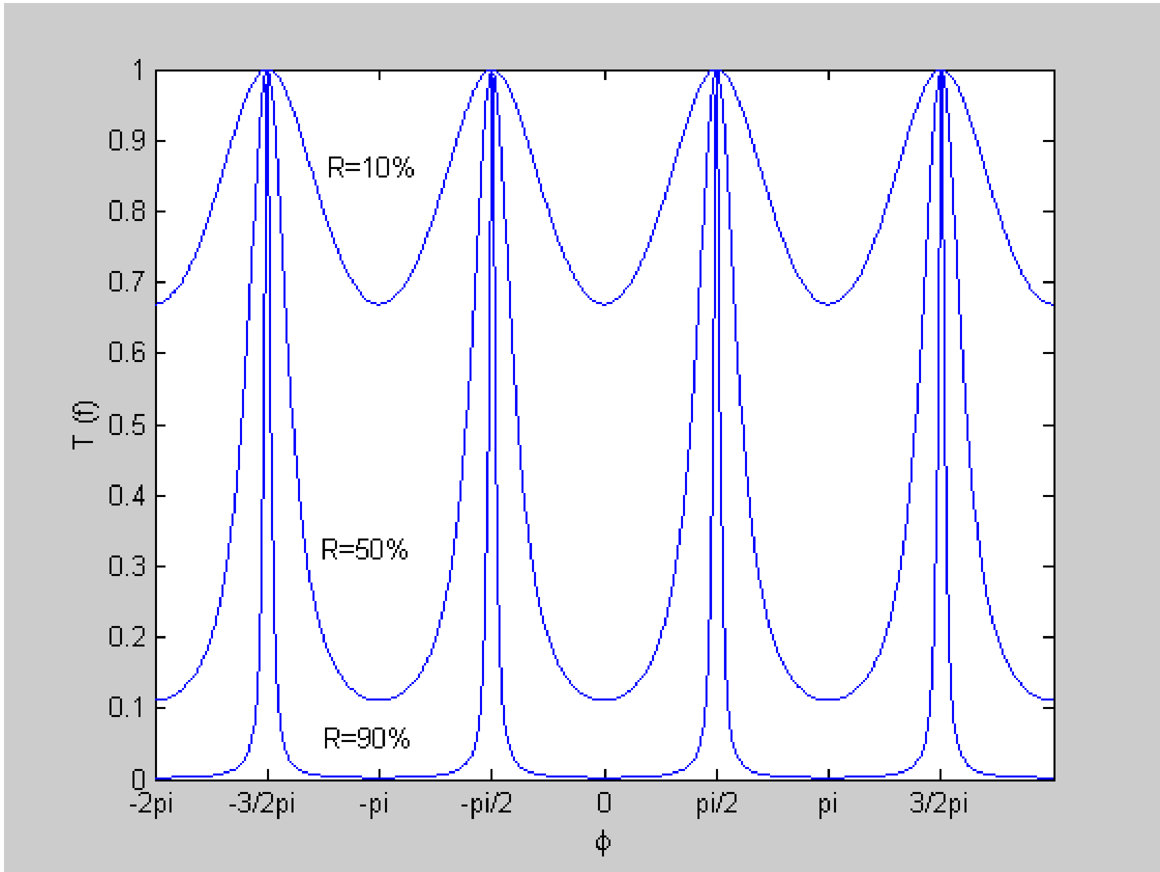

Fig. 13. The power transfer function of two reflector Fabry Perot filter.

The frequency difference between two adjacent frequency peaks is known as the tuning range or free spectral range, which is given by

$$FSR(Hz) = \frac{c}{2n_f L} \tag{52}$$

where $c = 2.9979 \times 10^8 m/\sec$. For example, given an index of 1.46 with L = 1 mm and center wavelength of 1550 nm, the FSR is 102.669 GHz.

The 3-dB bandwidth is often called the full width at half maximum (FWHM) which is given by

$$FWHM(Hz) = \frac{c}{2nL}\frac{1-R}{\pi\sqrt{R}} \tag{53}$$

The most important performance parameter for Fabry Perot filter is the finesse [19] *F* which expresses the sharpness of the filter response relative to the repeat period and is related to the maximum number of channels which can be implemented in an optical communication system. The finesse is given by

$$F = \frac{FSR}{FWHM} = \frac{\pi\sqrt{R}}{1-R} \tag{54}$$

To obtain high finesse and a narrow transmittance peak so that a large number of channels can be implemented, R should be as high as possible [20].

CHAPTER IV

DEVICE FABRICATION

A. Silicon Wafer Polishing Jig

The multireflector etalons which have been demonstrated experimentally in this Dissertation research are formed by placing equal-length sections of single mode fiber end-to-end. The fibers are mounted in a silicon jig and their ends are polished to achieve proper lengths with high-quality optical surfaces. Before polishing, a multilayer dielectric film is deposited on the end of each fiber section.

The fibers are held between two silicon wafers for polishing to the correct length. The first step is to cleave the Si to produce flat, parallel surfaces. This requires that the wafer be scored along a cleavage plane, as determined by the Miller indices [21]. Fig. 14 shows the three major Miller planes of silicon.

Each silicon wafer is produced by its manufacturer with a notch or a flat edge which represents its orientation, as illustrated in Fig.15.

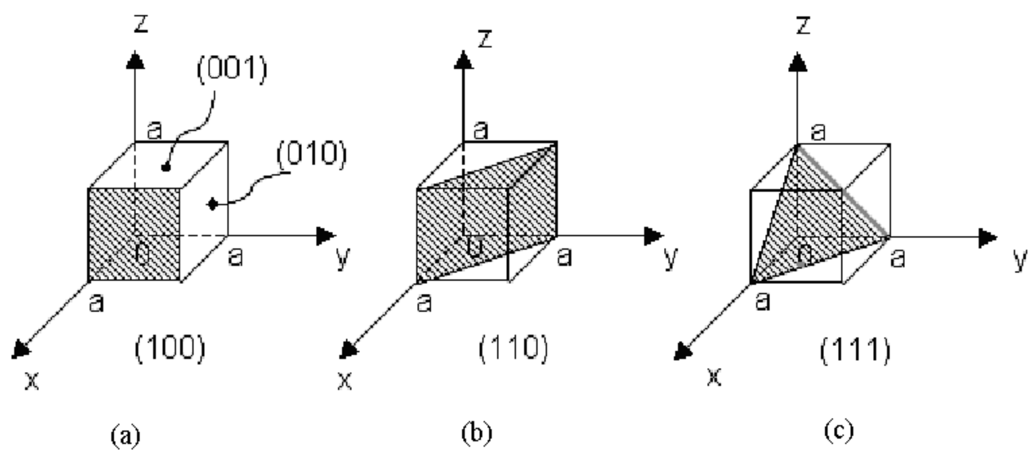

Fig. 14. Three major Miller planes of silicon.

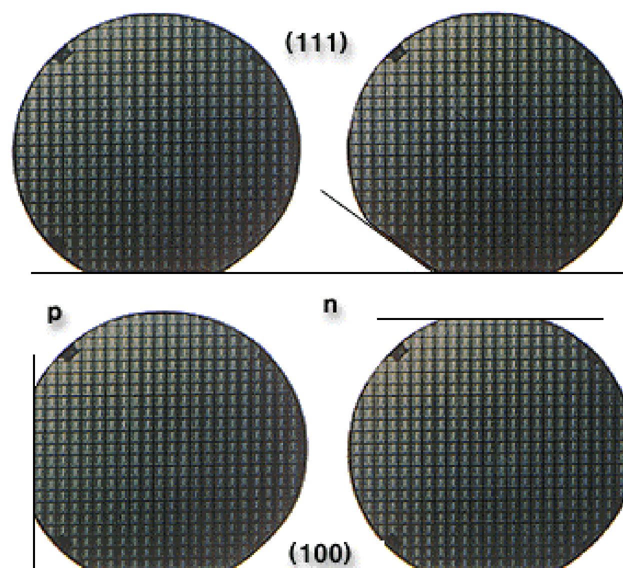

Fig. 15. Silicon wafers with two different orientations.

According to the Miller's plane orientation, silicon wafers with (100) orientation are chosen, which will produce cleaved surfaces perpendicular to the large flat surfaces of the wafer [22].

A thickness of 1 mm was chosen for the wafers, as it was found that thinner wafers tend to chip during the polishing process due to the high stress to which the wafer is subjected. After testing different wafer sizes, 6-inch-diameter wafers were selected. The depth of grooves on the silicon wafer were chosen to accommodate the 125μm(0.005") diameter of the fibers to be polished. These grooves were cut perpendicular to the cleaved edges of the wafer with a 0.003" dicing saw blade.

Because of mechanical friction between a blade and wafer during the cutting process, the grooves are widened to slightly greater than the 0.005" fiber diameter. Control of the groove depth is also important. If a fiber dips into the groove too far, the top cover cannot hold the fiber properly. Fig.16 illustrates a cleaved Si wafer with sawn grooves.

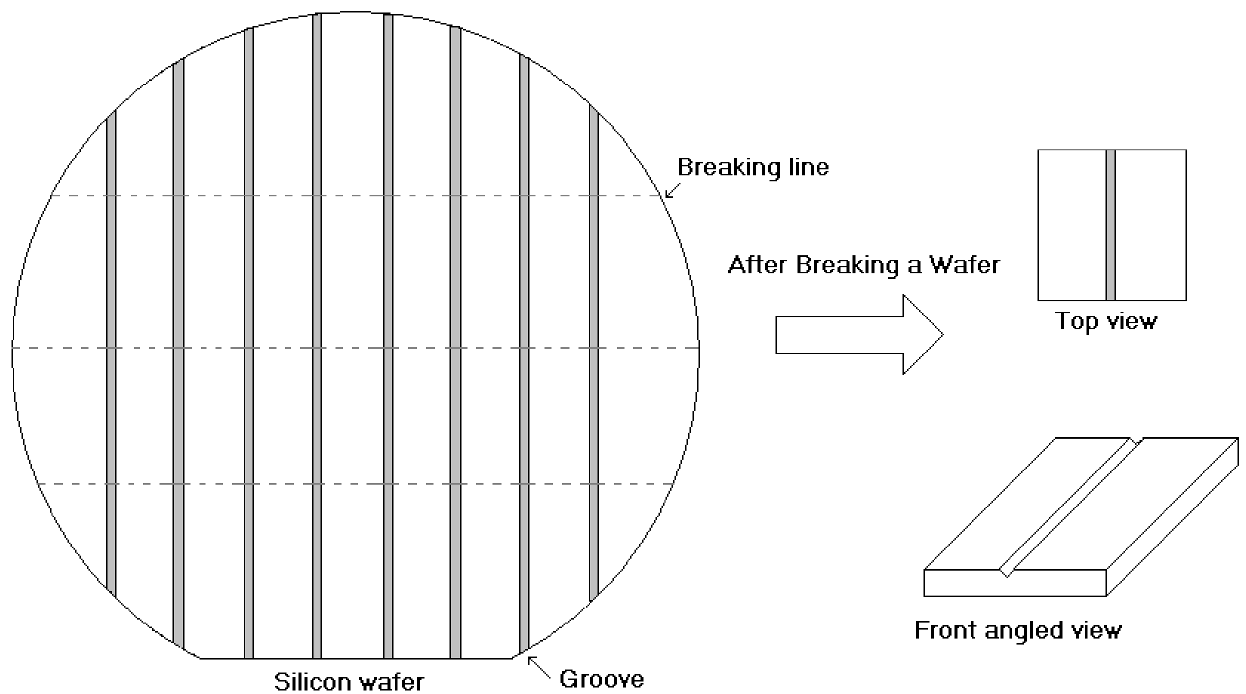

Fig. 16. A polishing jig after grooving on the silicon wafer.

This cover prevents the fiber from moving inside the groove during the polishing process which produces strong frictional forces. It is also important that the polishing surface be flat, since an angled fiber end surface might cause a significant performance degradation of the filter. The polishing jigs are illustrated in Figs. 17 and 18.

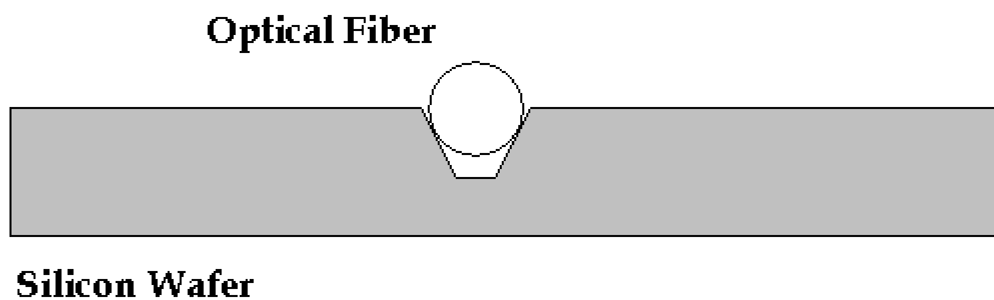

Fig. 17. A silicon wafer with a fiber positioned in a groove.

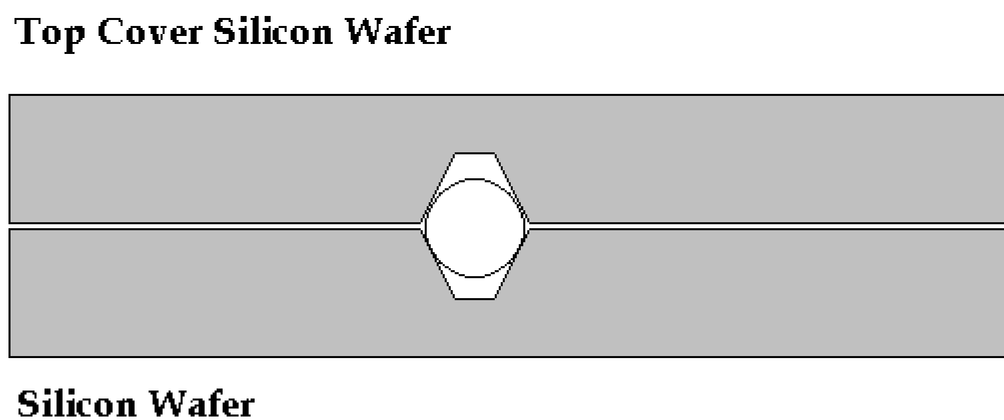

Fig. 18. A polishing jig with top cover in place.

B. Coating Materials

Thin film dielectric mirrors generally consist of alternating layers of two different coating materials, one with a high index of refraction and the other with a low index.

Characteristics of coating materials for multilayer thin film reflectors which should be considered include their optical properties, adhesion forces, hardness, and resistance to temperature, humidity, and chemicals [23]. The difference in index between the two materials is also important, because, according to equation (11), the greater the difference between refractive index n_1 and n_2, the higher the reflectance.

Characteristics of some dielectric coating materials are given in Table 2. In the visible and near-infrared spectral regions (0.4 -1.8μ), zinc sulfide and titanium dioxide are used as high-index materials and magnesium fluoride and silicon oxide as low-index materials. These materials exhibit strong molecular bonding on glass-based substrates [24] as well as low absorption loss over a wide range of wavelengths.

Table 2. The characteristics of some coating materials.

Material	Approximate index of refraction	Useful wavelength region(μ)
$NaAlF_2$	1.35	<0.2 – 10
MgF_2	1.38	<0.2 – 5
SiO_2	1.45	0.2 – 8
Al_2O_3	1.69	0.2 – 7
CeO_2	2.3	0.4 – 5
ZnS	2.3	0.4 – 15
TiO_2	2.3	0.4 – 12
Si	3.4	0.9 – 8
Ge	4.0	1.3 – 35

TiO_2 and SiO_2 are frequently used in combination, while ZrO_2 and Al_2O_3 are used in some cases [25].

There are two major classifications of deposition techniques, each having subclassifications, as shown in Fig. 19.

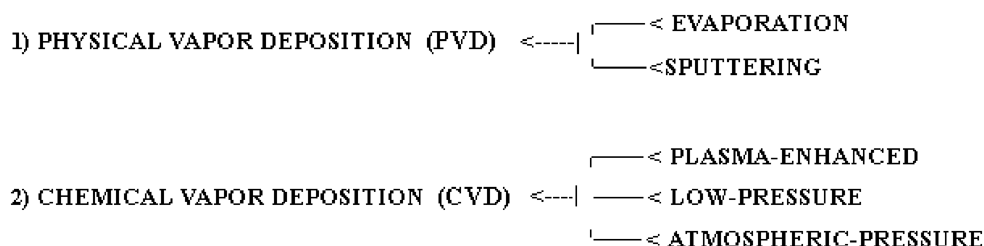

Fig. 19. Deposition techniques.

The film should be uniformly deposited over the surface, and the results should be repeatable. For for volume production, deposition must be inexpensive with a large throughput. Most dielectric thin films can be produced by sputtering, which consists of bombarding the target of the desired material with ions in a vacuum chamber so that atoms are ejected to collided with and stick to the substrate [15]. This method can be especially useful for refractory materials that are difficult to handle by other means. Alternatively, vacuum evaporation in which the target is evaporated by thermal or electron beam heating and deposited onto the substrate, can be applied. The refractive indexes of TiO_2 and SiO_2 thin films are shown as a function of wavelength in Fig. 20 [12].

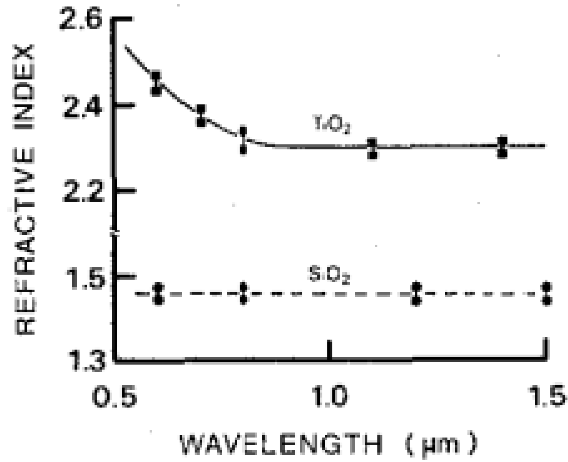

Fig. 20. Refractive indices of TiO_2 and SiO_2.

The refractive index of the SiO_2 thin film is approximately constant at 1.46 within the 0.5 - 1.5μm wavelength region. In the designand calculations, the refractive indexes of TiO_2 and SiO_2 are taken to be 2.3 and 1.46 respectively, as appropriate for the 1.5 μm spectral region.

C. Coating Thickness of Each Dielectric Thin Film

The reflectance of the mirrors depends on the thicknesses of the layers as well as the refractive index difference $n_1 - n_2$. The reflectance of a single layer thin film of refractive index n_2 and thickness t between semi-infinite layers of index n_1 is calculated from

$$R = A_{12}{}^2 + A_{23}{}^2 + \left(2A_{12}A_{23}\cos\left(\frac{4\pi\, n_2\, t}{\lambda} \right) \right) \tag{55}$$

where R is the reflectance and λ is the wavelength of the light.

$$A_{12} = \frac{n_1 - n_2}{n_1 + n_2} \tag{56}$$

$$A_{23} = \frac{n_2 - n_3}{n_2 + n_3} \tag{57}$$

As seen in equations (56) and (57), if the refractive index of a substrate is less than the refractive index of a film, the parameter A_{12} is negative. Therefore, for maximum reflectance, the cosine term should equal –1, which requires that

$$\frac{4\pi n_2 t}{\lambda} = (2m+1)\pi, \; m = \text{integer} \tag{58}$$

The thinnest film which gives a maximum reflectance is

$$t = \frac{\lambda}{4 n_2} \tag{59}$$

The thickness of the film is a quarter of the wavelength of the light in the film. This is illustrated by the plot of reflectance vs. film thickness for two different wavelengths in Fig. 21.

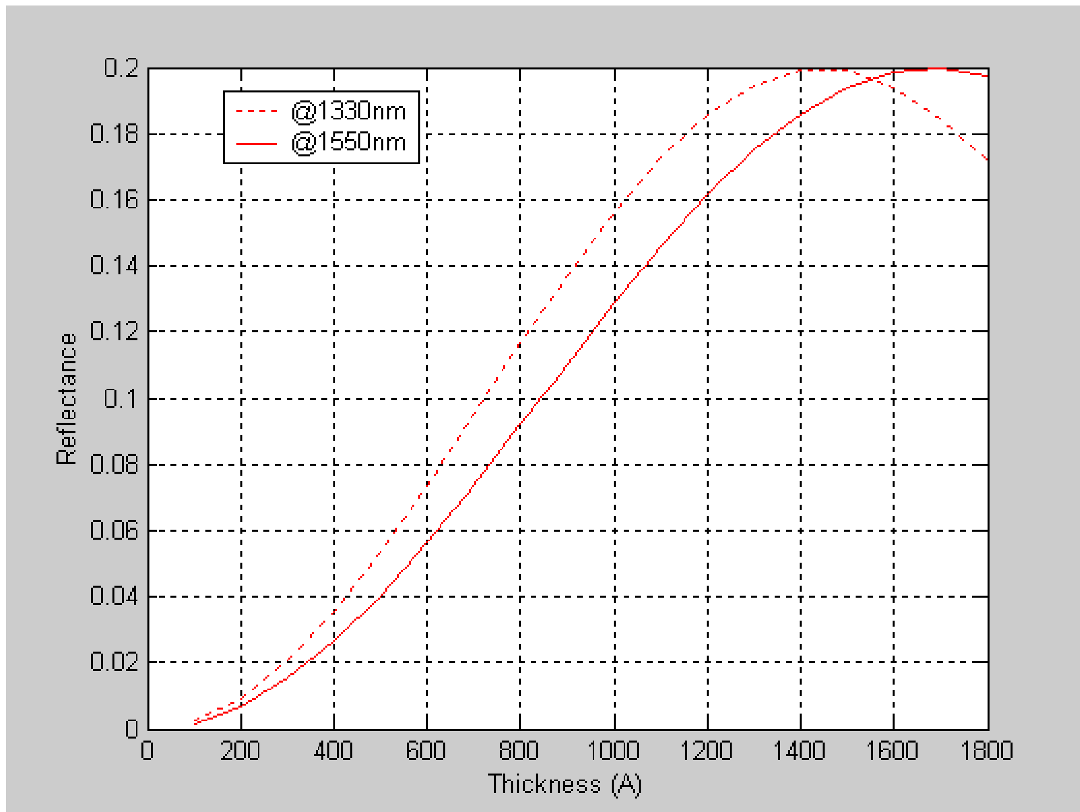

Fig. 21. Dependence of reflectance on film thickness for a film of index n_2=2.3 sandwiched between regions of index n_1=n_3=1.46.

In the filter described in this Dissertation, the thickness for the single layer dielectric thin film is 800Å, which corresponds to approximately a 10% reflectance value.

D. Polishing

In preparing for the polishing process, a fiber to be polished is aligned inside a sawn groove in a Si wafer using a precision micro positioning moving stage as in Fig. 22. The fiber is slid inside the groove until the desired length is contained within the groove, as determined by monitoring with a microscope. After alignment, the fiber and adapter are bonded together using epoxy.

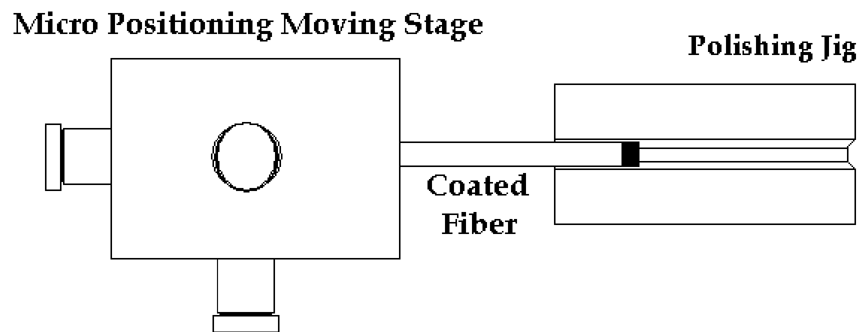

Fig. 22. A diagram of aligning a fiber in the polishing jig.

A Model 69-3000 FIBRMET optical fiber polisher, shown in Fig.23, is employed for the polishing process.

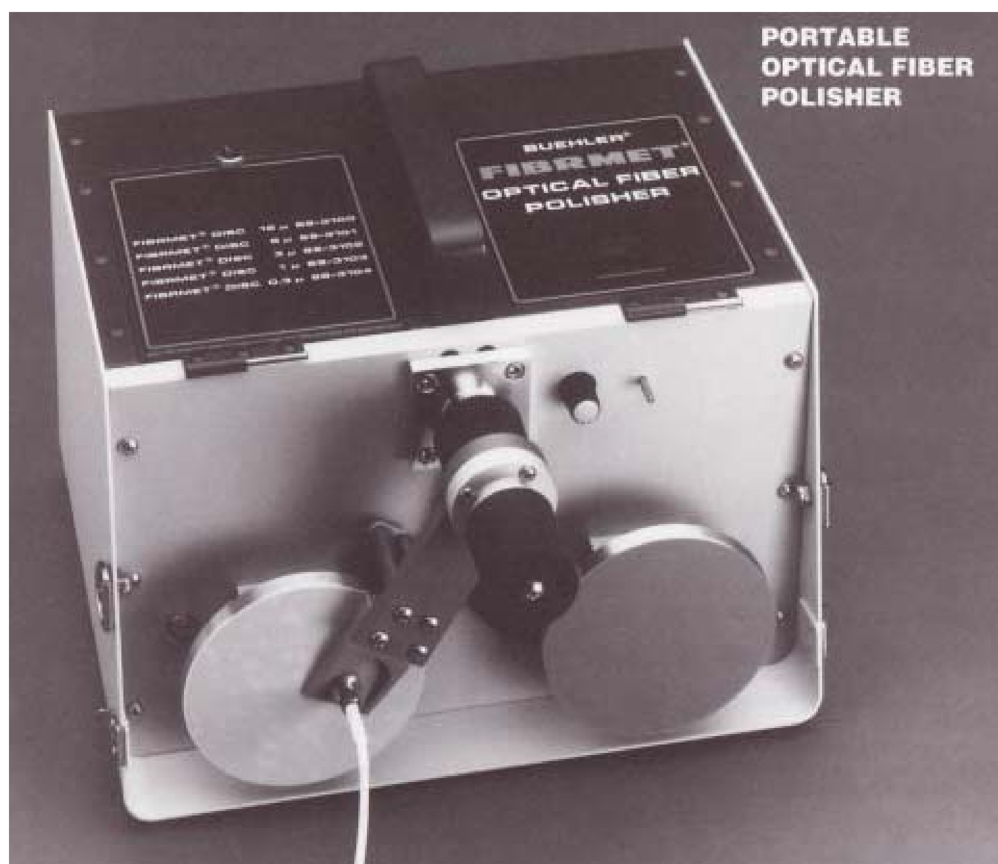

Fig. 23. 69-3000 FIBRMET optical fiber polisher from Beuhler Ltd.

The polishing jig is inserted and securely attached to the polishing adapter holder. Four abrasive discs are successively applied to polish the fiber end surface.

First, very coarse 12 micron grain size abrasive discs are used to remove the epoxy around the fiber. Then 3 micron abrasive discs are applied for smoothing. The end surface is checked by microscopic observation to see if the visible scratches have been removed. If the surface is found to be satisfactory, fine polishing is commenced; otherwise, the 3 micron polishing step is repeated.

The fine polishing process is started by applying 1 micron grain size abrasive discs, and completed by applying 0.3 micron abrasive discs. This finishing process takes a little bit longer than the other processes and also requires the application of water to achieve a satisfactory end surface. Silicon wafers are hard materials, so the length loss of the polishing jig is very small. This length loss has been taken into account during positioning the fiber on the polishing jig.

E. The Silicon V-groove

To produce a multireflector etalon, equal-length single mode fiber sections, each of which has a dielectric mirror on one end, are aligned end-to-end in a Si v-groove. Silicon v-groove chips have been used for precise alignment between fibers and opto-electronic devices such as laser diodes, active waveguides, passive waveguides, optical switches, and arrayed waveguide gratings (AWGs) for high coupling efficiency and fiber pigtailing [26]. Precision alignment of the crystal orientation gives good uniformity of a silicon v-groove opening and angles. These silicon v-grooves can be integrated with passive or active waveguide devices on a single chip. The characteristics of the silicon v-groove, which were donated by LG Electronics Institute of Technology, are shown in Fig. 24 and Table 3.

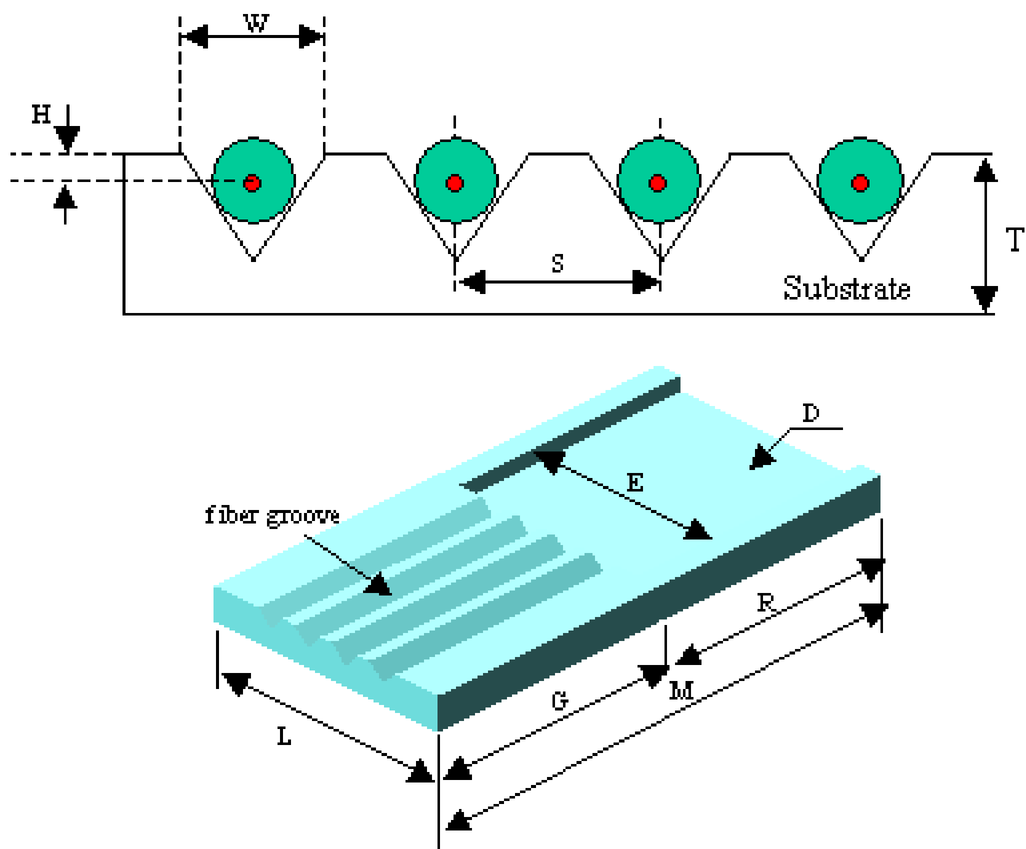

Fig. 24. A diagram of the silicon v-groove.

Table 3. Specifications of the silicon v-grooves.

Fiber spacing(S) (μm)	250<±0.5
Groove width(W) (μm)	200<±1.0
Substrate thickness (T) (μm)	625<±20
Groove length (G) (μm)	5150<±20
Chip width (L) (μm)	3000<±20
Chip length (M) (μm)	9000<±20
Core height (H) (μm)	33.2<±0.5
Strain relief area length(R) (μm)	3850<±20
Strain relief area width (E) (μm)	2400<±5
Etching depth (D) (μm)	157<±3

The polished sets of fibers with desired reflectance values are aligned in a silicon v-groove to assemble an optical fiber Fabry Perot filter. Pertinent parameter of the Corning single mode from which relate to mode mismatch loss are : core diameter = 8.2μm, numerical aperture = 0.14, cladding diameter = 125±1μm, core cladding concentricity ≤ 0.5μm. Before putting the fibers in the v-grooves, refractive index matching material is applied inside the v-groove to eliminate the air gap between adjacent fiber ends as shown in Fig. 25. Additional unplanned reflections form air-fiber interfaces will degrade the response characteristic of the optical filter. Aligning fibers inside the silicon v-groove is very crucial and requires very careful manipulation of the fibers.

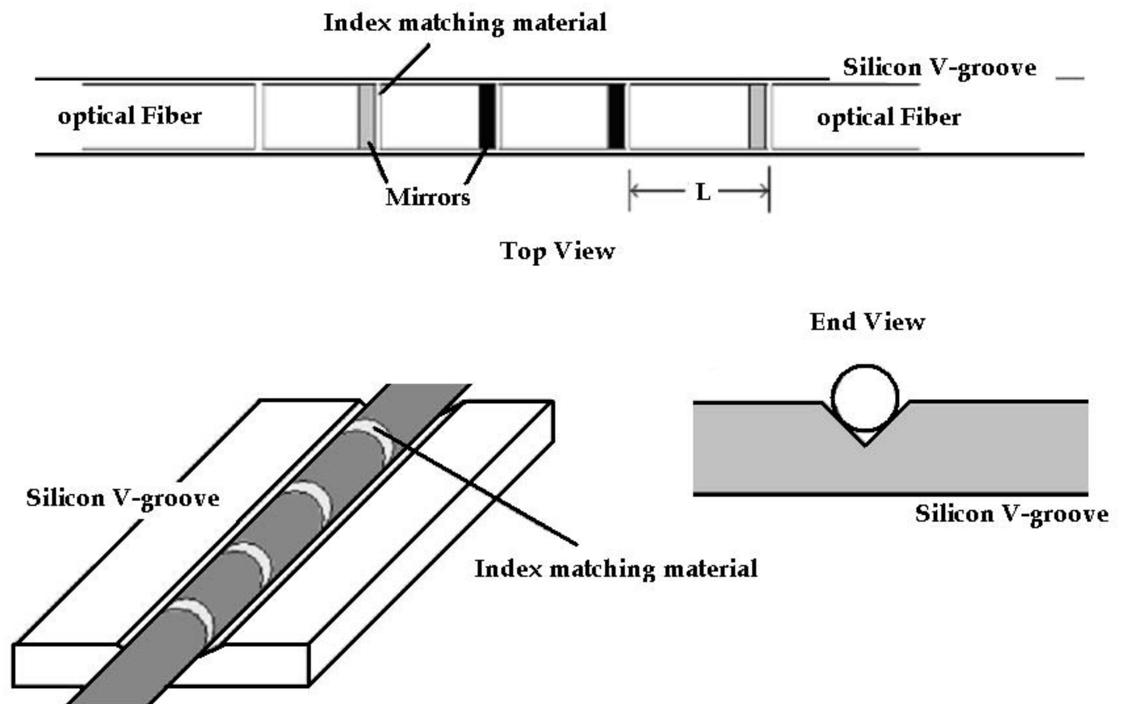

Fig.25. Aligning fibers inside the silicon v-groove.

F. Setup for Optical Testing of the Filters

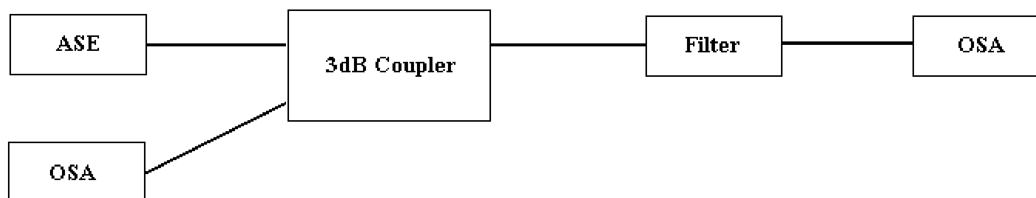

Fig. 26. The optical test setup.

Amplified Spontaneous Emission (ASE) light from Erbium-Doped Fiber Amplifier (EDFA) is employed as a broadband light source to measure the spectral response of the filter [27] in Fig. 26. An Erbium doped fiber based ASE source emits amplified spontaneous light in the C-band (1530-1560nm) or in the L-band (1560-1610nm). Therefore such sources are ideal for characterizing optical components such as isolators, circulators, gratings, add/drop multiplexers for dense wavelength division multiplexing (DWDM) systems [28].

Light from the Amplified Spontaneous Emission (ASE) light source is launched into the 2×2 3-dB fiber optic coupler which divides the optical power of the light source equally. The fiber which transmits light from the coupler to the filter is cleaved and aligned with the input port of the silicon v-groove.

After applying an index matching material inside the silicon v-groove, four mirrors (low reflectance, high reflectance, high reflectance, and low

reflectance) separated by equal fiber lengths are aligned within the v-groove as depicted in Fig. 27. A photograph of the entire optical test setup is shown in Fig.28.

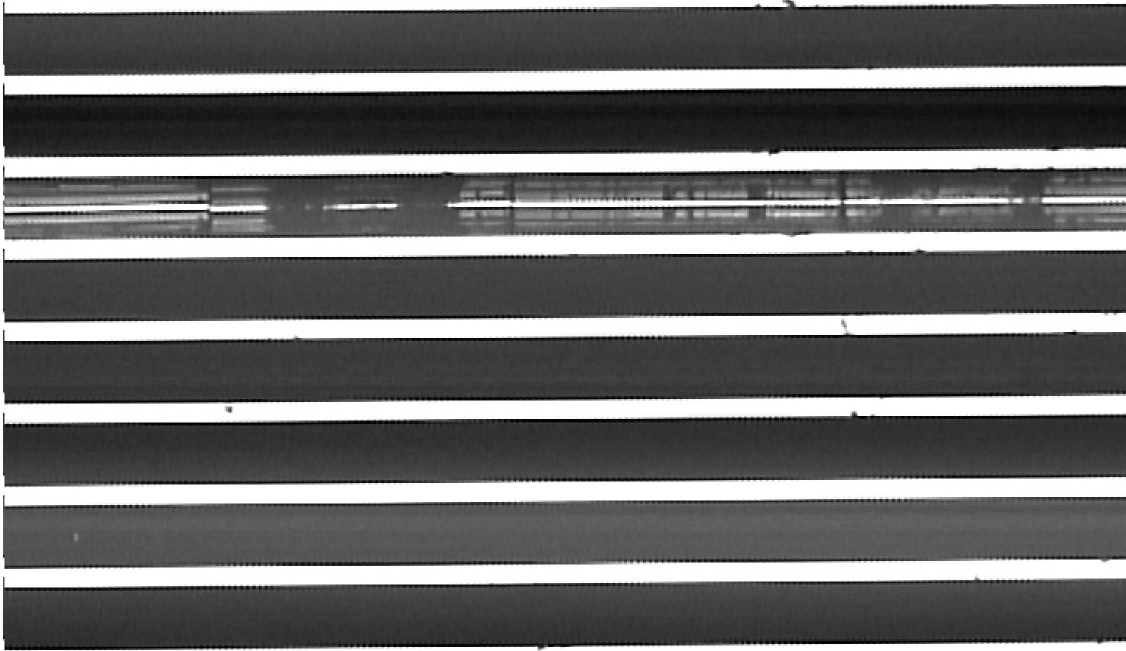

Fig. 27. Fibers inside the silicon v-groove.

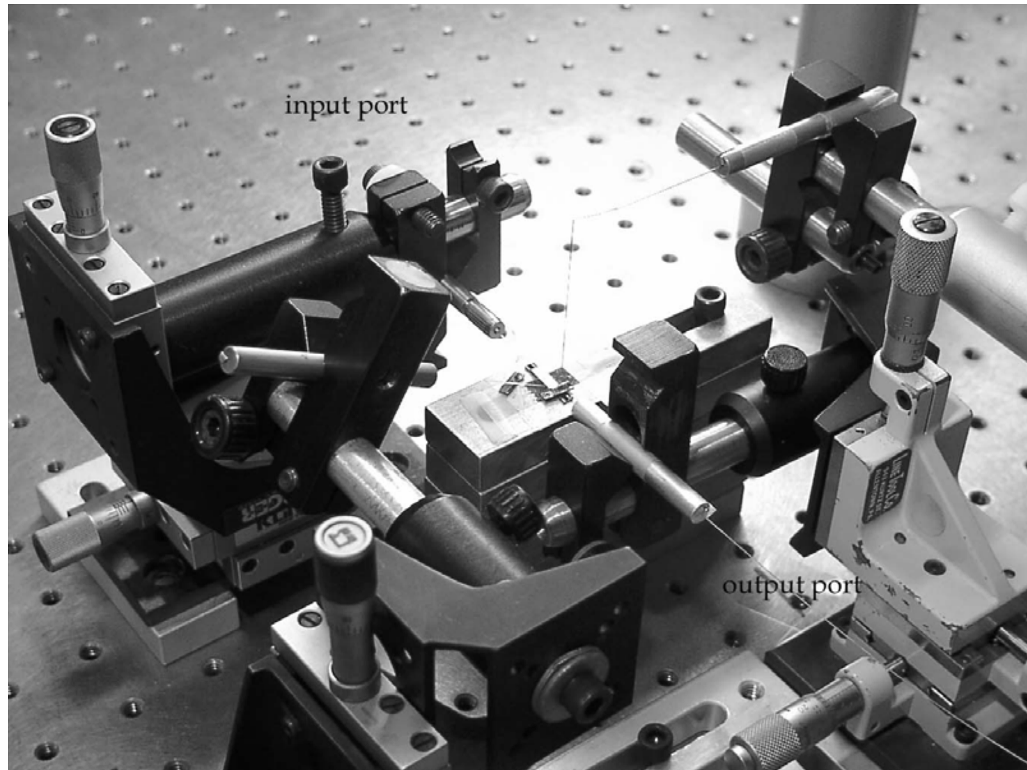

Fig.28. The experimental setup.

The transmission spectrum is measured using an Anritsu MS9710C Optical Spectrum Analyzer (OSA). The spectrum of the ASE light source measured with the OSA is shown in Fig. 29.

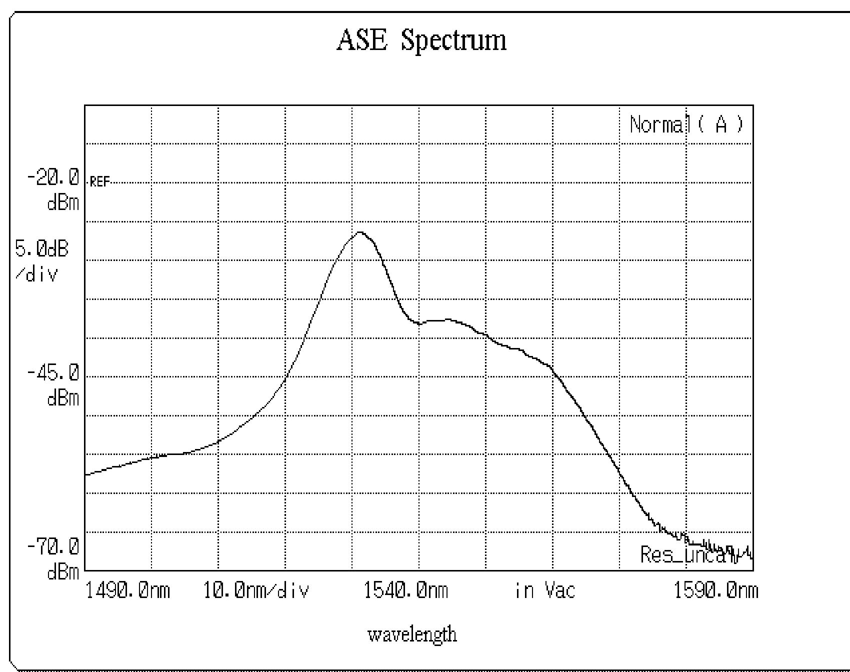

Fig. 29. ASE output Spectrum.

CHAPTER V

OPTICAL TESTING AND DATA ANALYSIS

A. Characterization of the Fiber Sections

As a prerequisite to constructing a multireflector filter, optical characterization is carried out for each fiber section, half of which have 50% reflectors on one end, and the rest of which half have 10% reflectors. In both cases the fiber-air Fresnel reflectance from the uncoated fiber end is 3.5%.

It is particularly important that the fiber sections be precisely matched in length, since the length of each etalon determines the Free Spectral Range (FSR) of the filter. It is also important that the reflectors have low excess optical loss, and that the dielectric reflectance values be close to the design values of 10% and 50%.

Each individual fiber section is aligned inside a v-groove. No index matching material is applied because the reflection from the interface between air and the fiber end is needed so that the measured reflection and transmission spectra can be used to characterize the etalon.

The Free spectral range (FSR) can be easily measured using the optical spectrum analyzer by measuring wavelength or frequency intervals between two adjacent spectral peaks. One way to determine FSR is to count the

number of spectral peaks over a given wavelength range from transmittance spectra like the one in Fig. 30.

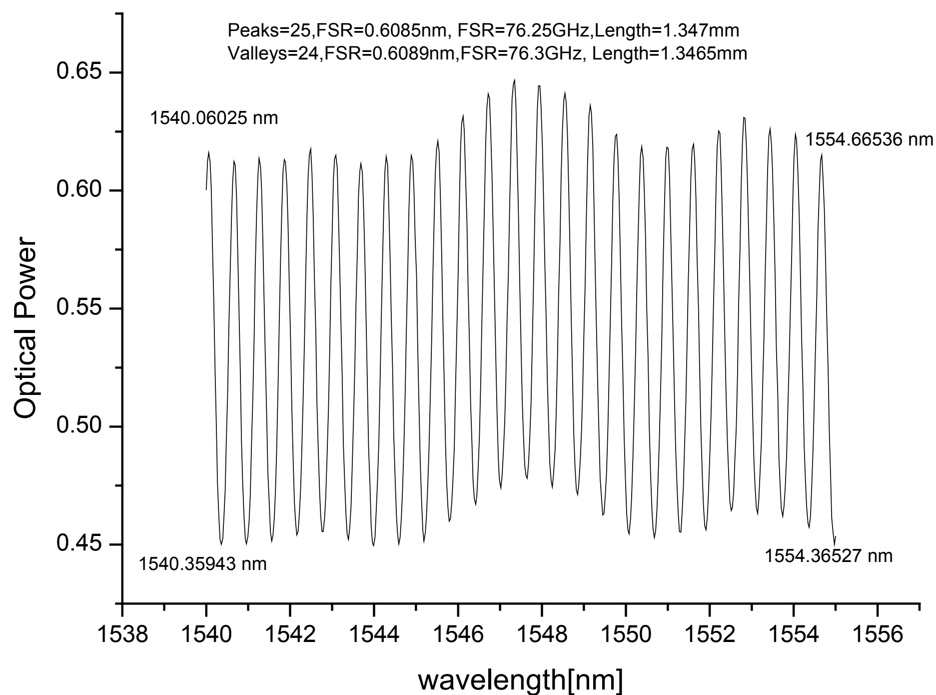

Fig. 30. Transmittance spectrum for a single fiber section with a 10% mirror on one end and a Fresnel reflection of 3.5% from the other end.

The Free spectral range (FSR) and physical length of each etalon are given by

$$FSR(Hz) = \frac{\#of\ peaks - 1}{\Delta \nu} \tag{60}$$

$$FSR(Hz) = \frac{\#of\ valleys - 1}{\Delta \nu} \tag{61}$$

where Δν and $\Delta\lambda$ represents the frequency range over which the spectrum is measured in using equation (52), the length of each etalon is calculated as

$$L = \frac{c}{2\, n\, FSR} \tag{62}$$

with *n* the refractive index of the fiber.

The measured characteristics of 8 fiber sections are summarized in Table 4, based on analysis of the spectra in Figs. 31-38.

Table 4. Characteristics of fiber sections.

Part No.	Theoretically 10% reflectors				Theoretically 50% reflectors			
	R	Loss	FSR	Length	R	Loss	FSR	Length
1	9.6 %	- 1.09 dB	Peaks = 76.95GHz Valleys= 76.86GHz	Peaks = 1.335mm Valleys= 1.337mm	49 %	- 1.06 dB	Peaks = 78.16GHz Valleys= 78.22GHz	Peaks = 1.315mm Valleys= 1.3134mm
2	9.5 %	- 1.12 dB	Peaks = 76.87GHz Valleys= 76.62GHz	Peaks = 1.34mm Valleys= 1.33mm	49.6 %	- 1.17 dB	Peaks = 76.7GHz Valleys= 76.6GHz	Peaks = 1.33mm Valleys= 1.34mm
3	9.6 %	- 1.5 dB	Peaks = 76.56GHz Valleys= 76.55GHz	Peaks = 1.34mm Valleys= 1.34mm	48.6 %	- 1.28 dB	Peaks = 77.3GHz Valleys= 77.4GHz	Peaks = 1.329mm Valleys= 1.327mm
4	10.6 %	- 1.2 dB	Peaks = 76.25GHz Valleys= 76.3GHz	Peaks = 1.347mm Valleys= 1.3465mm	51.3 %	- 1.04 dB	Peaks = 83.97GHz Valleys= 83.994GHz	Peaks = 1.22mm Valleys= 1.22mm

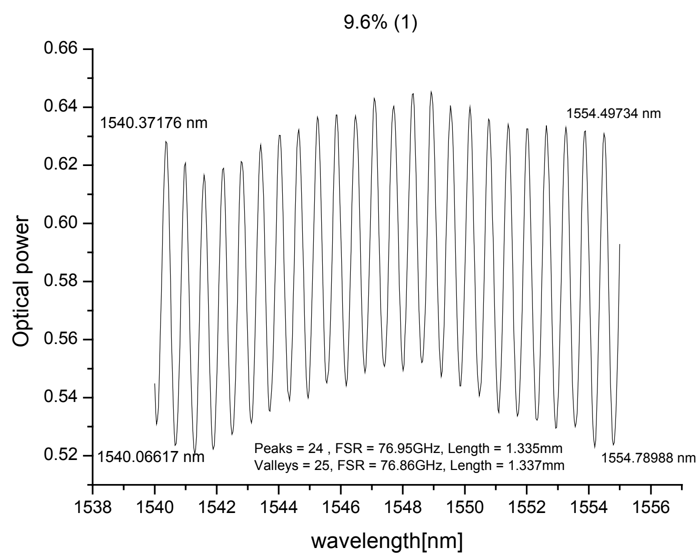

Fig. 31. Transmittance spectrum of fiber section 1 with, R=9.6%.

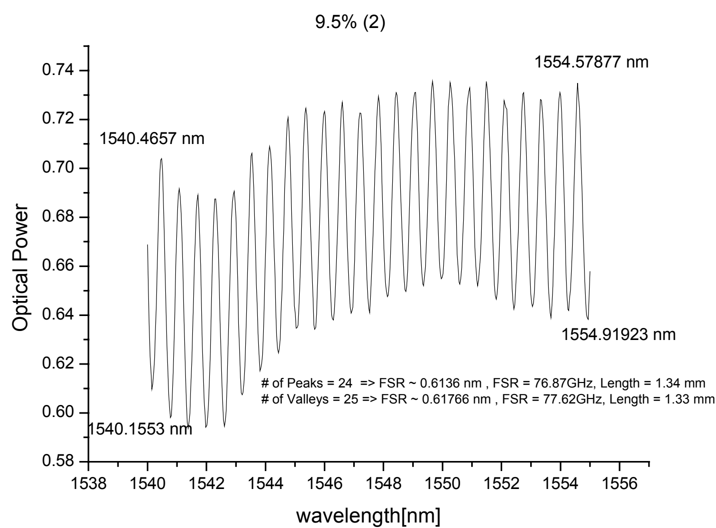

Fig. 32. Transmittance spectrum of fiber section 2 with, R=9.5%.

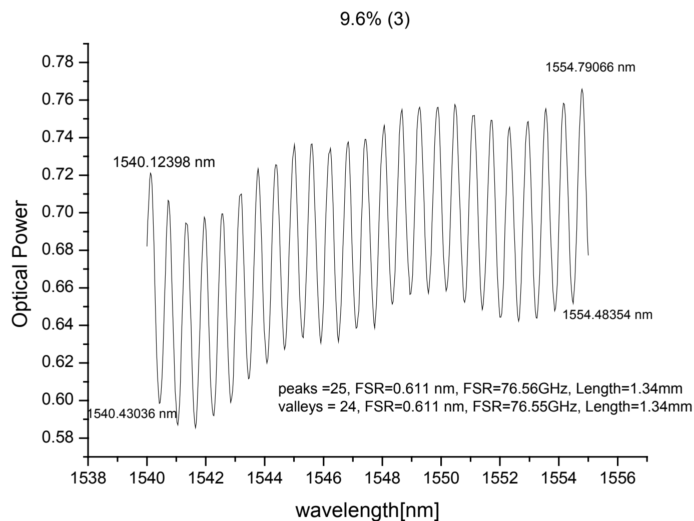

Fig. 33. Transmittance spectrum of fiber section 3 with, R=9.6%.

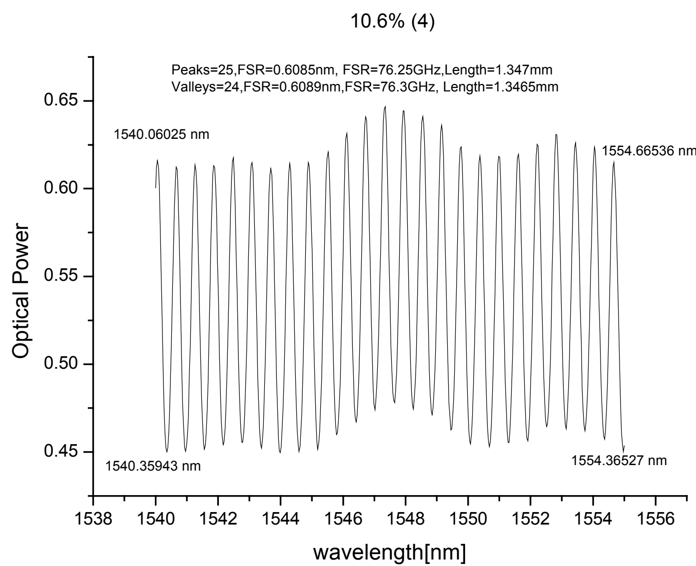

Fig. 34. Transmittance spectrum of fiber section 4 with, R=10.6%.

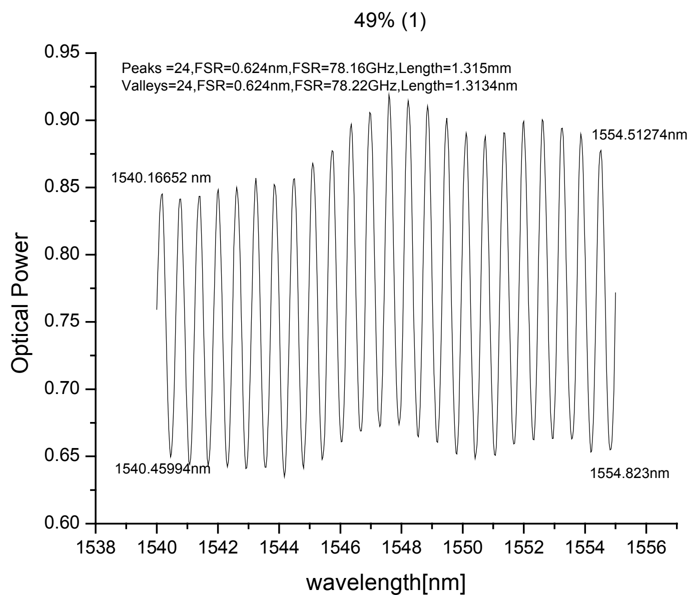

Fig. 35. Transmittance spectrum of fiber section 1 with, R=49%.

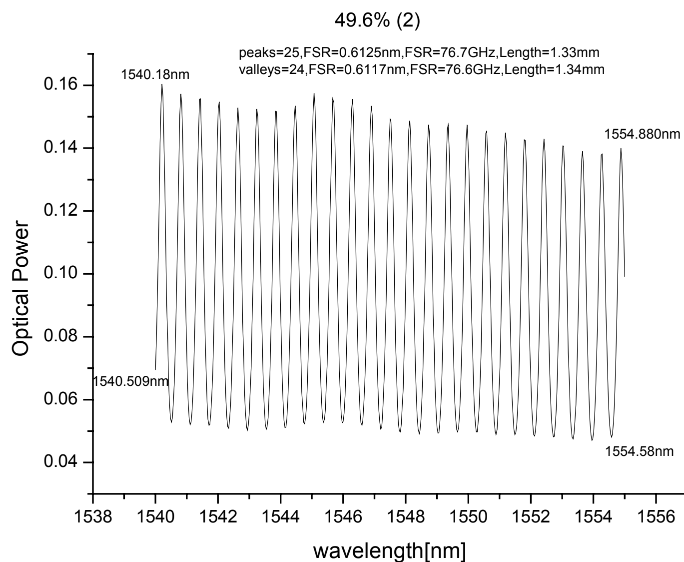

Fig. 36. Transmittance spectrum of fiber section 2 with, R=49.6%.

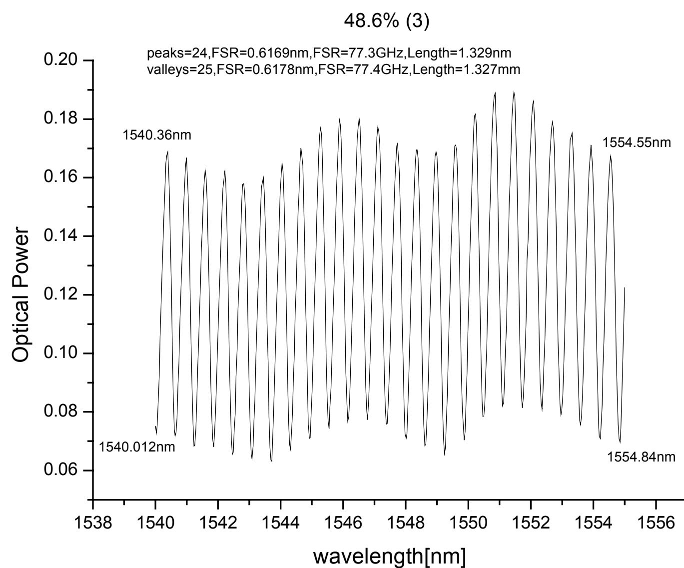

Fig. 37. Transmittance spectrum of fiber section 3 with, R=48.6%.

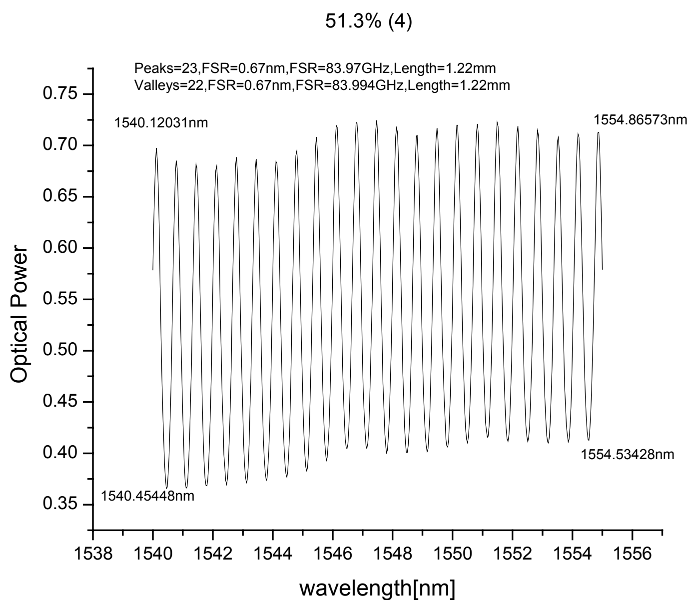

Fig. 38. Transmittance spectrum of fiber section 4 with, R=51.3%.

Based on the spectral data in Figs. 31-38 as summarized in Table 4, the combination of fiber sections with reflectances 9.6%(1), 49.6%(2), 48.6%(3), and 9.5%(2) is selected for assembly of a four-reflector etalon.

The Fringe visibility,

$$V = \frac{P_{Max} - P_{Min}}{P_{Max} + P_{Min}} \tag{63}$$

is another indication of the spectral quality of the fiber sections.

The dependences of V on wavelength for two fiber sections, one with a 9.6% mirror and the other with a 49% mirror, are plotted in Figs. 39 and 40.

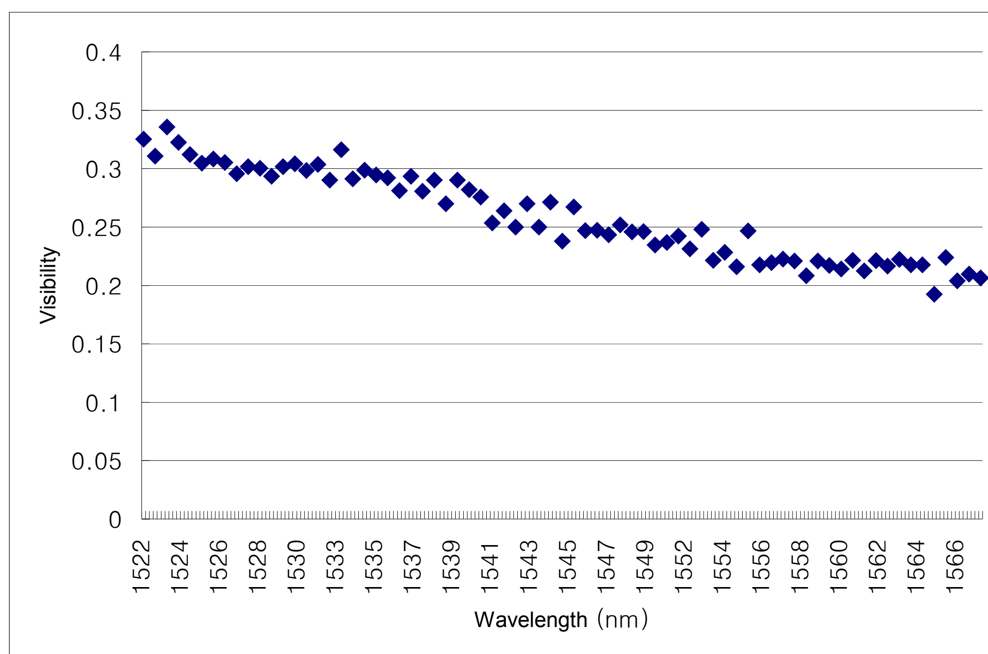

Fig. 39. Visibility test of a fiber with a 9.6% reflector on one end.

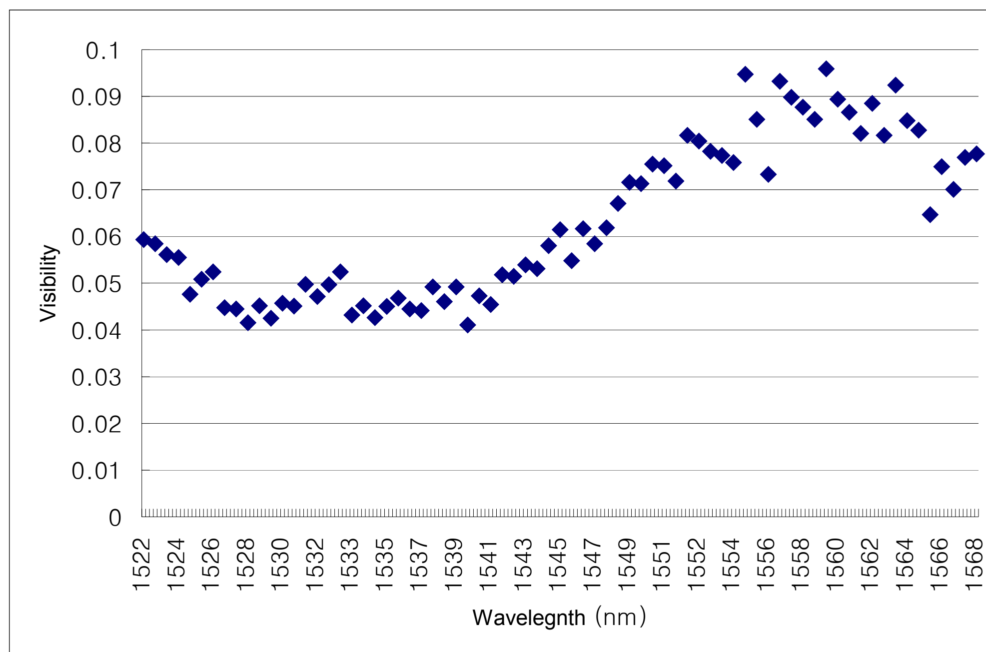

Fig. 40. Visibility test of a fiber with a 49% reflector on one end.

B. Characteristics of Multireflector Etalon

The four-reflector etalons were assembled one reflector at a time. Transmittance spectra were measured for N=2 (one 10% reflector and on 50% reflector), for N=3 (one 10% reflector and two 50% reflectors), and N=4 (one 10% reflector, two 50% reflectors, and one 10% reflector)

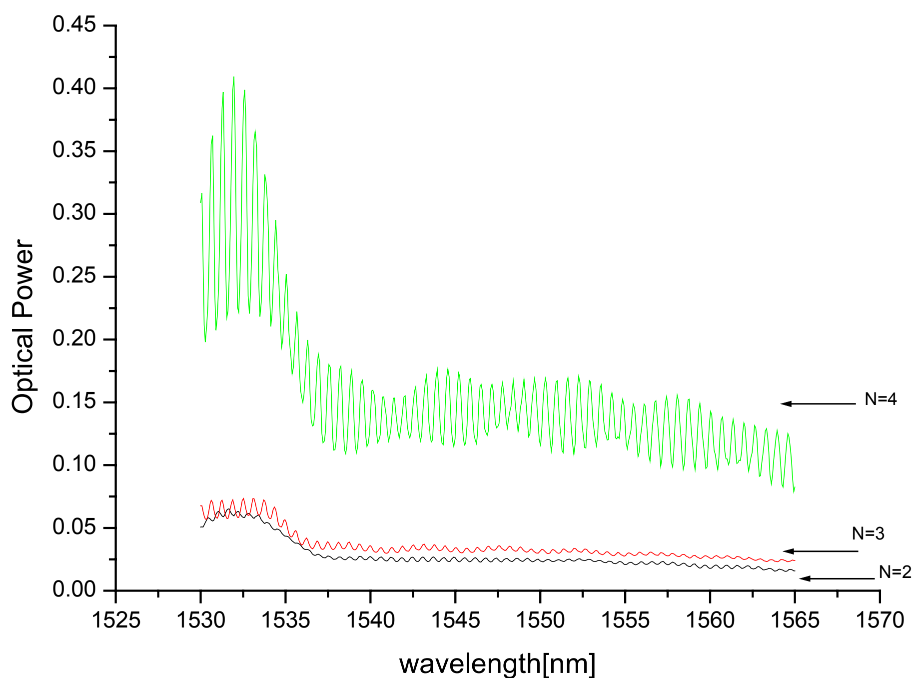

Fig. 41. Transmission spectra for N=2, 3, and 4 over the C-band (1530-1560nm).

As shown in Fig. 41, the greater the number of reflectors, the greater the fringe visibility, as expected. High resolution spectra for three- and four-mirror etalons are shown in Fig. 42 with optical power plotted on a logarithmic scale.

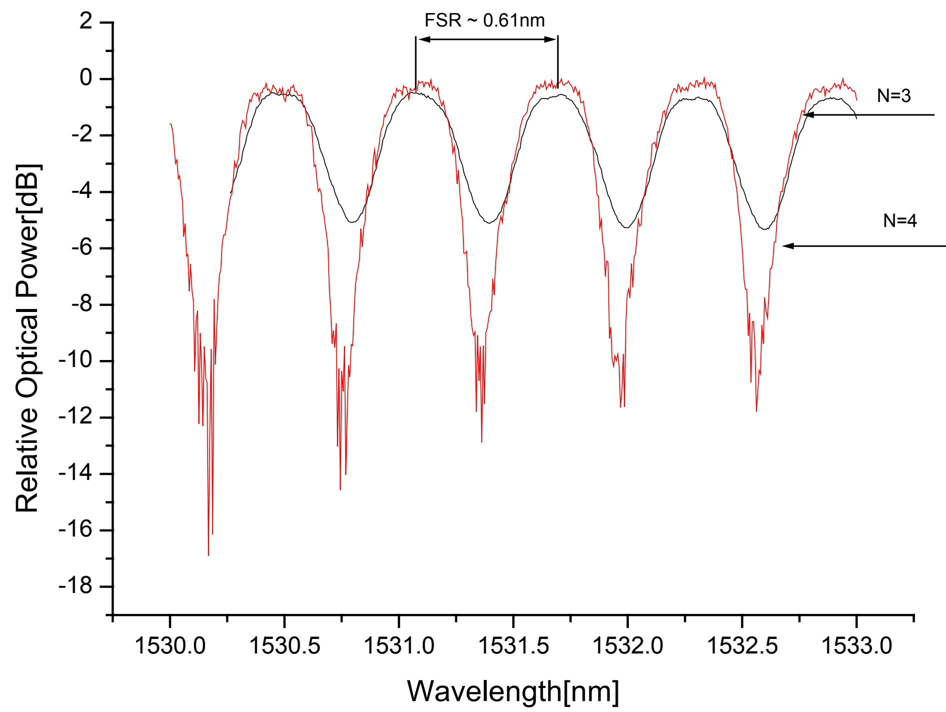

Fig. 42. Transmittance specta for N=3 and 4,

with optical power plotted on a logarithmic scale.

As shown in Fig. 42, the top of the passband of N=4 is flatter than the passband of N=3, as expected.

When an index matching material is not applied in the silicon v-groove, undesired additional reflections occur at the uncoated fiber ends. This degrades the filter response spectrum, as shown in Fig. 43.

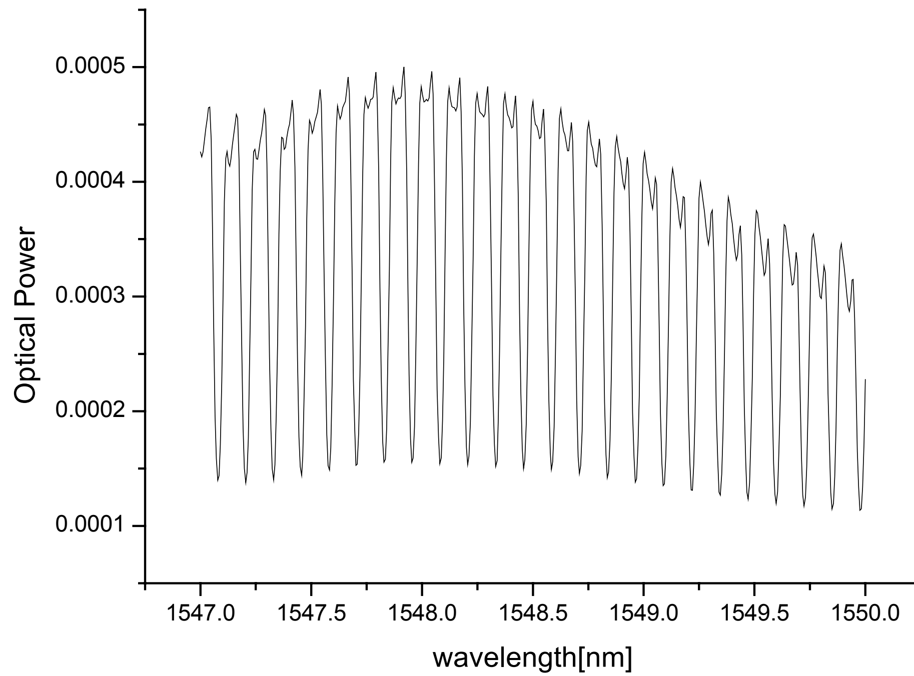

Fig. 43. The transmission spectrum without index matching.

Finally, the experimental transmittance spectrum for N=4 is compared with the spectrum calculated from equation (44) as shown in Fig. 44.

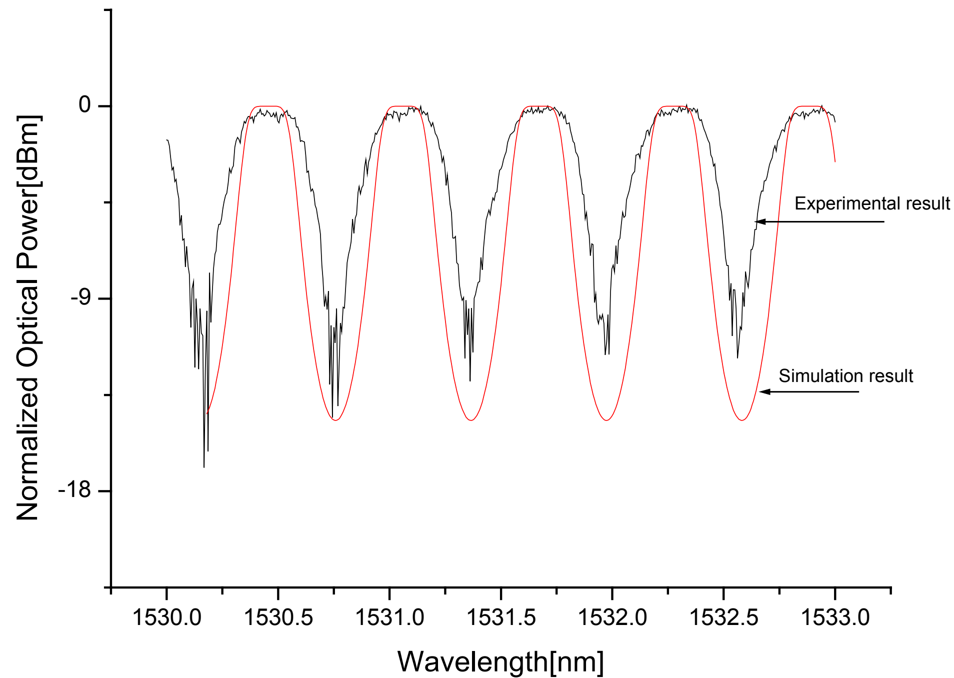

Fig. 44. Comparison between calculated and observed transmittance spectra for N=4.

The measured spectrum of N=4 multireflector Fabry Perot bandpass filter has approximately FSR = 77GHz, Depth =13dB, and FWHM=47GHz. The FSR is almost identical with the values measured for the individual fiber sections used in assembling the 4-mirror etalon.

The transmission spectrum of the N=4 filter over the entire C-band (1530 ~ 1560nm) is shown in Fig. 45. The fringe visibility of the filter

transmission spectrum is almost uniform, which means that this multireflector Fabry Perot bandpass filter design can be applied to a C-band optical communication system.

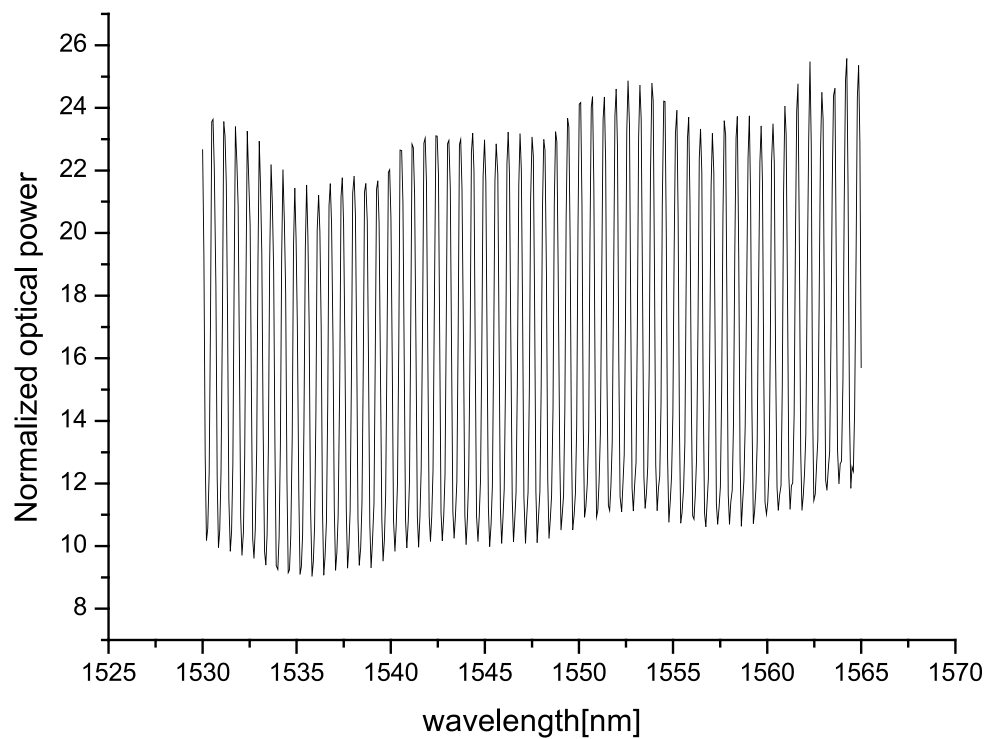

Fig. 45. A transmission spectrum over entire C-band (1530~1560nm).

Measured transmittance and reflectance spectra are compared in Fig. 46 for the four-reflector etalon.

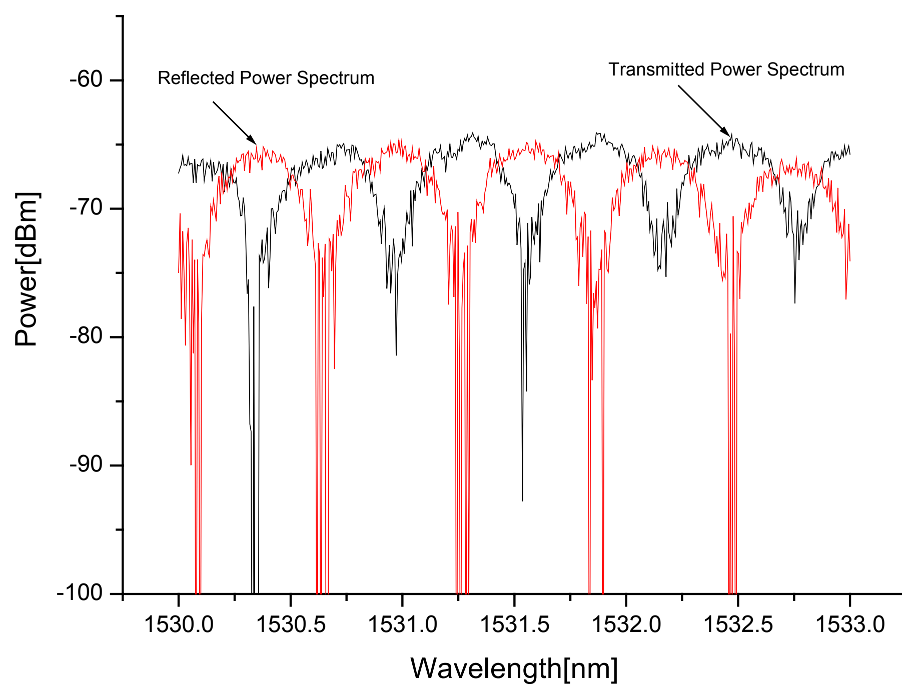

Fig. 46. Measured transmission and reflection spectra for four-mirror etalon.

C. Temperature Tuning

Thermal tuning of the fiber filter has been investigated and the result is shown in Fig. 47. The silicon v-groove was mounted on a thermoelectric cooler module, which was used to change its temperature over the range 3^0 C to 26^0 C. The transmittance peak wavelength was observed to shift by 0.34 nm. The predicted wavelength shift is given by

$$\Delta\lambda = \lambda\left(\frac{1}{nL}\frac{d}{dT}(nL)\right)\Delta T \tag{64}$$

where $\frac{1}{nL}\frac{d}{dT}(nL)$ is the thermal coefficient of optical length for a single mode silica fiber using the measured value $\frac{1}{nL}\frac{d}{dT}(nL) = 8\times10^{-6}/^{\circ}\mathrm{C}$ [29], the calculated wavelength change is 0.285 nm.

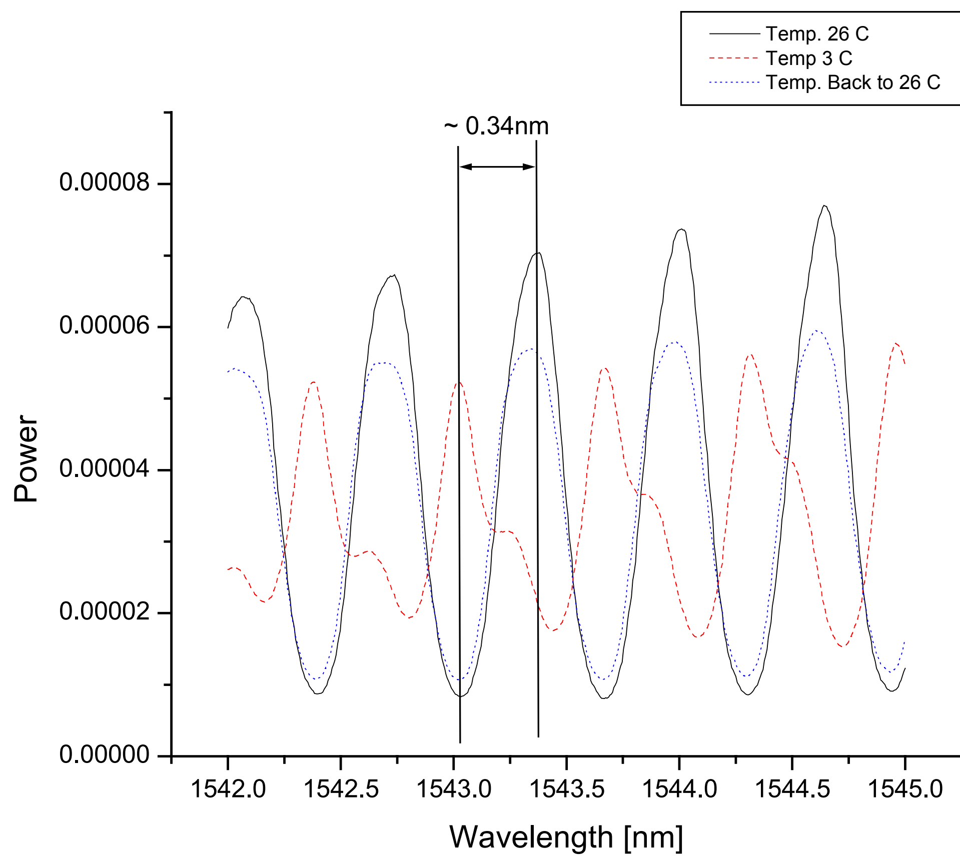

Fig. 47. Temperature tuning of the spectral response.

CHAPTER VI

CONCLUSIONS

An all fiber multireflector spectral filter has been investigated experimentally. A four-mirror etalon with reflectance values near 50% for the two inner mirrors and 10% for the outer mirrors was implemented experimentally.

This multireflector etalons were produced by aligning equal-length fiber sections with dielectric mirrors deposited on the end in a silicon v-groove. The lower reflectance mirrors are single TiO_2 layers deposited on the end of a single mode fiber, while the higher reflectance mirrors are alternating TiO_2/SiO_2 layers. Individual fiber sections 1.33 mm in length were produced by polishing in a silicon polishing jigs.

After positioning a fiber inside a groove of the polishing jig using a precision micro positioner, four polishing steps with successively finer grit were applied and bonding it in place, to produce high quality fiber end surfaces.

Prior to assembling the four-mirror etalon, transmittance spectra of individual fiber sections were characterized. An analysis of these spectra yielded information on the lengths and optical loss of these sections, as well as the reflectances of the mirrors deposited on their ends.

Based on these data, four length-matched sections were chosen for assembly of the four-mirror etalon. Refractive index matching material was

applied to provide optical continuity between adjacent fiber sections. Measured transmittance spectra for this multireflector etalon were compared with calculated spectra.

Thermal tuning of the multireflector etalon was also investigated. A 0.34 nm wavelength shift was observed for a 23^0 C temperature change, in agreement with the predicted wavelength shift.

CHAPTER VII

RECOMMENDATIONS

Multireflector spectral filters can be implemented by aligning a large number of equal-length fiber sections with dielectric mirrors deposited on their ends in a silicon v-groove. Some factors which can be taken into account in achieving high-performance commercialized products are discussed below.

The length of etalons for the filters can be reduced to achieve higher Free Spectral Range (FSR) than the 77GHz characteristic of the present devices. This can be controlled by a micro-positioning stage. A mass polishing technique is needed for mass production and to achieve polished fibers which are very closely matched in length as required to achieve the best spectral characteristics for the filters.

Individual mirrors with reflectances much higher than those used in the present work will be needed to reduce the transmittance bandwidth of the filters. This will require that the number of TiO_2 and SiO_2 layers be increased.

It is important that the fiber sections are well aligned inside the silicon v-groove. The larger number of fiber sections, the greater the excess optical loss due to positional mismatch of the ends. This misalignment causes a performance degradation of the spectral filters. Another method to align the fiber sections would utilize tubes, such as zirconia ceramic ferrules used in demountable optical fiber connectors. The ferrules can be cut in half horizontally to produce a groove in which the fiber sections can be aligned.

REFERENCES

[1] C.A. Bracket, “Dense WDM networks,” *Optical Communication, 1988. ECOC 88. Fourteenth European Conference on (Conf. Publ. No.292)*, 11-15, 1988.

[2] B. Ortega, J. Capmany, D. Pastor, and R.I. Laming, “Experimental demonstration of an ultraselective and tunable optical bandpass filter using a fibre grating and a Fabry-Perot,” *Electronics Letters*, vol.33, pp.669-671, 1997.

[3] J. Capmany, B. Ortega, and D. Pastor, ” Fibre optic bandpass filter with subpicometre bandwidth using a fibre grating and two fibre Fabry-Perot filters,” *Electronics Letters* , vol.33, pp. 1970-1972, 1997.

[4] B. Ortega, J. Capmany, and J.L. Cruz, ”Wavelength division multiplexing all-fiber hybrid devices based on Fabry-Perot's and gratings,” *Journal of Lightwave Technology*, vol.17, pp. 1241 –1247, 1999.

[5] J. Stone, L.W. Stulz, and A.A.M. Saleh, “Three-mirror fibre Fabry-Perot filters of optimal design,” *Electronics Letters*, vol.26, pp. 1073-1074, 1990.

[6] D. Marcuse and J. Stone, “Fiber-coupled short Fabry-Perot resonators,” *Journal of Lightwave Technology*, vol.7, pp. 869-876, 1989.

[7] H. de Stadt and J.M. Muller, ”Multimirror Fabry-Perot interferometers,” *J. Opt. Soc. Amer. A*, vol.2, pp.1363-1370, 1985.

[8] H.F. Taylor, “Design of multireflector resonant bandpass filters for guided wave optics,” *Journal of Lightwave Technology*, vol.19, pp. 866-871, 2001.

[9] H.F. Taylor, “Principles and applications of fiber-optic Fabry-Perot sensors,” *Lasers and Electro-Optics*, 1998. CLEO 98. Technical Digest. Summaries of papers presented at the Conference on , 3-8 May 1998.

[10] C.E. Lee, C.E., W.N. Gibler, R.A. Atkins, and H.F. Taylor, “In-line fiber Fabry- Perot interferometer with high-reflectance internal mirrors,” *Journal of Lightwave Technology,* vol.10, pp. 1376-1379, 1992.

[11] C.E. Lee and H.F. Taylor “Fiber-optic Fabry-Perot temperature sensor using a low-coherence light source,” *Journal of Lightwave Technology,* vol.9, pp. 129-134, 1991.

[12] J. Minowa and Y. Fujii, “Dielectric multilayer thin-film filters for WDM transmission systems,” *Journal of Lightwave Technology,* vol.1, pp. 116-121, 1983.

[13] J. Stone and L.W. Stulz "FiEnd filters: Passive multilayer thin-film optical filters deposited on fibre ends," *Electronics Letters*, vol.26, pp.1290-1291, 1990.

[14] L.F. Stokes, "Optical-fiber filters for wavelength division multiplexing," *IEEE Circuits and Devices Magazine*, vol.12, pp. 49-50, 1996.

[15] H.Demiryont and J.R.Sites, "Effects on oxigen in ion-beam sputter deposition of titinium oxides," *J.Vac.Sci.Technol.*, vol.A2(4), pp.1457-1460, 1984.

[16] J.D. Rancourt, "Introduction to optical thin films," *SPIE*, pp. 7-10, 1996.

[17] G.R. Fowles, *Introduction to modern optics*, Second Edition, New York: Dover Publications Inc., 1975.

[18] P.E. Green, Jr., *Fiber optic networks*, New York: Prentice Hall, 1993.

[19] S. Doucet, R. Slavik, and S.LaRochelle, "High-finesse large band Fabry-Perot fibre filter with superimposed chirped Bragg gratings," *Electronics Letters*, vol. 38, pp. 402 –403, 2002.

[20] C.M. Miller, "Characteristics and applications of high performance, tunable, fiber Fabry-Perot filters," in. *Proc. Electronic Components and Technology Conf.,* Atlanta, GA, May 1991.

[21] Wert andThomson, *Physics of Solids*, Second Edition, New York: McGraw-Hill, 1970.

[22] P. Van Zant, *Microchip Fabrication*, Third Edition, New York: McGraw-Hill, 1997.

[23] G. Hass and R. E. Thun, *Physics of Thin Films*, Volume 5, New York: Academic Press, 1969.

[24] S. Kaneko, M. Noda, K. Shibata, T. Aoyagi, H. Watanabe, T. Hatta, and K. Kasahara, "Novel fiber alignment method using a partially metal-coated fiber in a silicon V-groove," *IEEE Photonics Technology Letters*, vol.12, pp. 645 –647, 2000.

[25] L.Holland, *Vacuum Deposition of Thin film*, London: Chapman and Hall Ltd., 1966.

[26] T. Bricheno, H.F.M. Priddle, R.G. Peall, and D. Spear, "Packaging of optoelectronic devices with high coupling efficiency using silicon V-groove technology," *Optical Fiber Communication Conference and Exhibit, 1998. OFC '98.*, Technical Digest, pp. 349 –350, 1998.

[27] P.C. Becker, N.A Olsson, and J.R. Simpson, *Erbium-Doped Fiber Amplifiers,* New York: Academic Press, 1999.

[28] E. Desurvire and J.R. Simpson, "Amplification of spontaneous emission in erbium-doped single-mode fibers," *Journal of Lightwave Technology,* vol.7, pp. 835–845, 1989.

[29] C.E. Lee and H.F. Taylor, "Optical-fiber Fabry-Perot embedded sensor," *Optical Society of America*, vol. 14, pp.1225-1227, 1989.

APPENDIX 1

MAGNETRON SPUTTERING MACHINE

VENT SYSTEM

* Open nitrogen tank behind e-beam (set regulator to 5-10 psi)

* Open all three vent valves on the system

* Turn interlock power on

* Turn chiller on

* Turn turbo pump controller power on and press start (green light should be on; takes about 10 minutes to warm up)

* Check if DC or AC supply is connected to target; Connect as needed (DC line
has a blue sticker on it)

* Change target

* Back target out using hand crank

* Unscrew wing nuts to target chamber

* Open target chamber

* Unscrew 3 spring-loaded target bolts

* Remove target

* Load target

* Replace target sheath (make sure pin aligns with slot)

* Screw 3 spring-loaded bolts in until hand-tight

* Close target chamber and tighten wing-nuts

* Move target in using hand crank until chrome stud indicates desired distance

* Load/Unload sample (samples should already be mounted on a sample plate
  for loading)

* When venting is completed, open bell jar ("B.J." switch)

* Remove shroud and remove carousel

* Load (or unload) sample plate onto carousel

* Replace carousel and shroud

* Move carousel to down position (carousel switch)

* Close bell jar ("B.J." switch)

ROUGHING

* Turn roughing pump power on (switch on inside of front door, to the left)

* Close "chamber vent" valve

* Make sure foreline valve is open (valve is below chamber (black))

* Open roughing valve 1/2 turn (has yellow sticker on it)

* Make sure bell jar seals

* When pumping slows, open roughing valve all the way

* When roughing line reaches 150 microns (about 10 min.), close roughing valve

HIGH VACUUM

* Check that roughing line pressure < 150 microns, and that turbo pump

controller indicates normal operation

* If roughing valve has been closed, open high vacuum valve while monitoring fore-line pressure (slightly at first, then all the way)

* Turn on ionization gauge (10^{-4} range) and light filament

* Close remaining vent valves

* Degas for 5 minutes

* Pump as needed (until ionization gauge goes below $2x10^{-5}$)

PRE-SPUTTERING AND DEPOSITION

* Turn ionization gauge off

* Open outside gas valves

* Open inside gas valve (connected to target chamber)

* Set gases : SiO_2,TiO_2

Ar=8.2 sccm, O_2=4.9 sccm

* Let gases stabilize

* Turn on high vacuum gauge (TP Gauge Bell Jar switch)

**************************For AC operation***************************

* Turn AC supply on, making sure carriage is down

* Turn power adjust up to 100W or Maximum Power, whichever is first (if it won't work, see "trouble shooting" at the end of this procedure)

* Close high vacuum valve until plasma lights, then adjust it for desired pressure

* Tune (phase and load) until reflected power is minimized

* Set power as needed (see log book) and repeat previous step

* Raise carriage

* Adjust carriage position as needed

* Deposit as needed, monitoring current

* When finished, lower carriage and turn supply off

* Shut off gases (outside valves first, then inside valve)

* Close high vacuum valve and turn off TP Gauge Bell Jar switch

* Vent (see above)

* Press stop on turbo controller

* When turbo stops (takes about 8 minutes), turn turbo power off (remove sample while waiting for turbo pump to stop)

* Turn interlock off

* Turn chiller off

* Remove sample (see Load/Unload sample)

* Rough bell jar (see above)

* Turn off roughing pump

* Close nitrogen bottle behind e-beam

* Close all vent valves

TROUBLE SHOOTING:

If AC or DC power supply won't work, check interlocks:

1. Interlock and chiller on
2. Front and back doors closed all the way
3. Check water level in re-circulator; add DI water if needed

Parameters:

Deposition	Target	Target distance	Rate(Å /min)	Supply
SiO_2	Si	4″	30	AC
TiO_2	Ti	4″	12	AC

APPENDIX 2

DICING SAW MACHINE

1. Preparation mount surface in O-ring.

2.● Turn on 4 knobs/switches for saw :

1) Air knob under bench (ON)

2) Vacuum pump power switch under saw (ON)

3) Vacuum line switch (Flip up)

4) Water line valve (ON)

2. Measure resistance between blade and spindle.

3.● Turn on saw power (big red button).

4. Select program button (turn on monitor).

5.● Turn off program button.

6. Clean platform.

7. Turn spindle ON (wait for a stable condition).

8. Zero chuck.

9. Align mount substrate.

10.● Vapor lock wafer ON.

10. Press ALIGN (using a microscope, check parallel).

11. Cutting (check the bottle, water should be in the bottle during cutting process).

12. Shut down machine - Follow the steps marked ● in reverse order.

VITA

Mr. Jongseo Lee was born in Seoul, Korea in 1968. He received his B. S. degree from the Electrical Engineering Department of Myong-Ji University in 1996 and M.S. degree from the Electrical Engineering Department of Texas A&M University in 1998. He worked as a researcher at Daewoo Electronics Co., Ltd. in Korea. He began his master studies in electrical engineering at Texas A&M University in the fall of 1996. He joined the staff at the Electro-Optics Laboratory as a research assistant in June of 1997. He received his Ph.D. degree in electrical engineering at Texas A&M University in August 2003. His main interests of studies are fiber optic communications and networks. He can be reached at the following address:

Jongseo Lee

206-28 Jeonnong 4-Dong Dongdaemun-Gu

Seoul, 130-854, Korea

e-mail : jongseo_kaggie@hotmail.com